



**HAL**  
open science

# Bio-inspired wave breakers to reduce swell erosion in the Bay of Biscay using Computational Fluid Dynamics

Corentin Thomas, Victor Lieunard, Baptiste Oudon, Olivier Bain, Rejanne Le Bivic, Arnaud Coutu

## ► To cite this version:

Corentin Thomas, Victor Lieunard, Baptiste Oudon, Olivier Bain, Rejanne Le Bivic, et al.. Bio-inspired wave breakers to reduce swell erosion in the Bay of Biscay using Computational Fluid Dynamics. *Regional Studies in Marine Science*, 2023, 62, pp.102965. 10.1016/j.rsma.2023.102965 . hal-04099641

**HAL Id: hal-04099641**

**<https://normandie-univ.hal.science/hal-04099641v1>**

Submitted on 11 Jan 2024

**HAL** is a multi-disciplinary open access archive for the deposit and dissemination of scientific research documents, whether they are published or not. The documents may come from teaching and research institutions in France or abroad, or from public or private research centers.

L'archive ouverte pluridisciplinaire **HAL**, est destinée au dépôt et à la diffusion de documents scientifiques de niveau recherche, publiés ou non, émanant des établissements d'enseignement et de recherche français ou étrangers, des laboratoires publics ou privés.

1  
2  
3  
4  
5  
6  
7  
8  
9  
10  
11  
12  
13  
14  
15  
16  
17  
18  
19  
20  
21  
22  
23  
24  
25  
26  
27  
28  
29  
30  
31  
32  
33  
34  
35  
36  
37

# **Bio-inspired wave breakers to reduce swell erosion in the Bay of Biscay using Computational Fluid Dynamics**

**Corentin Thomas <sup>a</sup>, Victor Lieunard <sup>a</sup>, Baptiste Oudon <sup>a</sup>, Olivier Bain <sup>a</sup>, Rejanne Le Bivic <sup>a</sup>, Arnaud Coutu <sup>a b</sup>**

<sup>a</sup> *Institut Polytechnique UniLaSalle Beauvais, 19 rue Pierre Waguet 60000 Beauvais, France*

<sup>b</sup> *Corresponding author: [arnaud.coutu@unilasalle.fr](mailto:arnaud.coutu@unilasalle.fr), 19 rue Pierre Waguet 60000 Beauvais, France*

**LRH: Thomas, Lieunard, Oudon, Bain, Le Bivic and Coutu**  
**RRH: Bio-inspired Wave breakers**

38 Abstract

39

40 Coastal management is one of the main concerns of coastal countries. Sea level rise  
41 caused by climate change can accentuate coastal erosion. One of its principal causes,  
42 in France, is swell. Several solutions exist to limit the erosive effects of swell, including  
43 wave breakers. Their main issue is that they protect a limited area and they can  
44 increase the erosion downstream of the protected structures because of the cut in the  
45 longitudinal transport. Therefore, existing wave breakers can't be a long-term solution  
46 to the problem of coastal setback. This paper is a proof of concept on the idea of  
47 creating bio-inspired wave breakers that do not increase the erosion downstream but  
48 it also shows that all the bio-inspirations are not appropriate. Two types of bio-inspired  
49 wave breakers have been modeled on CatiaR2021X®. The first type is inspired by  
50 the Torquigener albomaculosus' nest. The second type is inspired by the mangroves'  
51 shape. Both shapes are known for slowing the seafloor current. The interaction  
52 between the wave breakers and the swell in the Bay of Biscay has been simulated with  
53 Xflow®2020. The experimental data needed to validate the simulations were provided  
54 by the scientific literature. Because the results of the control simulations and of the  
55 simulation with existing wave-breaker shapes coincided, the results of the other  
56 simulations have been considered as relevant too, even if test bench experiments will  
57 be performed later to deepen these results. The simulations' results have shown that  
58 the nest-inspired shapes are increasing the erosion in the non-protected areas. On the  
59 contrary, the mangrove-inspired wave breakers could be a possible improvement to  
60 slow the coastal setback in the Bay of Biscay. This study aims to give first results about  
61 the general interaction between geometrical shapes and swell, independently of the  
62 materials of the wave breakers.

63 Keywords

64

65 Biomimicry, Erosion, Lattice-Boltzmann Method (LBM), Wall-Modeled Large Eddy  
66 Simulation (WMLES), Coastal research.

67

68

69

70

71

72

73

74

75

76

77

78

79

## 80 1. Introduction

81

82 With climate deregulation and global mean sea level (GMSL) rising, managing the  
83 shorelines is one of the main concerns of coastal countries. GMSL has risen since  
84 1900 by about 21 cm, including 7 cm since 1993 (Hay *et al.* 2015, Church *et al.*, 2013).  
85 Scientists' predictions cover 6 scenarios (Low to Extreme) that show that sea level  
86 could rise from 30 cm to 250 cm by 2100 (Kopp *et al.*, 2014; Lacroix *et al.*, 2019; Miller  
87 *et al.*, 2013; Sweet *et al.*, 2017). On low-altitude coasts, this phenomenon could  
88 reinforce coastal erosion, and cause the loss of habitations, agricultural or natural  
89 surfaces. In France, for example, 270 km of coastline are eroding at a rate superior to  
90 50 cm/yr. (MilieuMarinFrance, 2020). One of the main causes of coastal erosion in  
91 France, is swell (Aubie and Tastet, 2000; Sabatier *et al.*, 2009; Migniot and Lorin, 1979).

92 This well-known problem has been studied for years. In France, between 1940 and  
93 1950, three structures had already been built to decrease coastal erosion (Boulet *et*  
94 *al.*, 2018) and coastline management is a major concern of political institutions (French  
95 Ministry of ecological transition, 2022). In the past century several solutions were tried,  
96 usually classified as soft or hard methods. Soft methods allow solutions to be  
97 integrated into their environment. They are reversible and are cheaper in the short,  
98 medium, and long term. According to Van Rijn (2011), they allow the sediment stock  
99 to regenerate. Hard solutions include building wave-breaker or rockfill. These solutions  
100 are expensive but durable. One problem of wave breakers is that they only protect a  
101 portion of the coastline and it induces hydraulic erosion downstream and upstream of  
102 the protected areas (Boulet *et al.*, 2018; Williams *et al.*, 2018). This erosion increase  
103 is a problem for large-scale coastal management because the aim is to protect the  
104 most eroded areas without eroding the other areas. This is why actual wave breakers  
105 can't be a long-term solution to coastal setback problem until a solution will not be  
106 found to make wave breakers that are not transferring erosion to other areas. Different  
107 studies cover the optimum wave breaker parameters to reduce the erosion behind the  
108 structure (Carpentier and Brosselard-Faidherbe, 1986; Delage, 1954; Massel and  
109 Gourlay, 2000; Toyoshima *et al.*, 1966) but few researches treat the question of finding  
110 how to not increase erosion in non-protected areas. In France, where multiple  
111 structures have been set up to reduce swell erosion, this recurrent problem doesn't  
112 help to find large-scale solutions to the coastal setback.

113 France's coastline is 5,853 km long and faces 4 different seas and oceans with different  
114 wave climates: North Sea, English Channel, Atlantic Ocean, and the Mediterranean  
115 Sea. The English Channel and the Mediterranean Sea are exposed to wind sea and  
116 short periods swell, while the Bay of Biscay, facing the Atlantic Ocean is exposed to  
117 energetic and moderate-to-long period swells (Dodet *et al.*, 2019). This is explained by  
118 the fact that swell energy depends on the wind speed and on the water surface in  
119 contact with the wind, called the fetch. Studying a sand beach in the Bay of Biscay is  
120 relevant to quantify the efficiency of the solutions to coastal erosion in an energetic  
121 swell context. One of the possible solutions could be biomimicry.

122 Scientists used biomimicry and bio-inspiration for a long time to solve various  
123 problems. In 1903, the brothers' Wright plane was inspired by a pigeon flight (Cho and

124 [Wood, 2016](#)). Nowadays, shark skin is an inspiration for performant swimming suits  
125 ([Wen et al., 2014](#)). It is important to understand that biomimicry isn't a goal but a way  
126 to find innovative solutions to modern problems. In the wilderness, there are several  
127 examples of natural or biological structures that reduce sea currents' impacts. The  
128 discovery in 2012 of the *Torquigener albomaculosus* nest near the Japanese coast  
129 has inspired multiple studies. This circular 2 m large structure reduces the speed of  
130 the current in its centre ([Kawase et al., 2013](#); [Kawase et al., 2017](#); [Matsuura., 2015](#)).  
131 Another inspiration could be the mangroves root system that has been known for a  
132 long time for slowing sea current and consequently, helping in coastal stabilization  
133 ([Horstman et al., 2014](#); [Hong Phuoc and Massel, 2006](#); [Thom, 1967](#); [Van Santen et al., 2007](#)).  
134 Both shapes could be an inspiration to create wave breakers. Because  
135 seafloor current speed is directly linked to erosion ([Everett et al., 2019](#); [Migniot and  
136 Lorin,1979](#)), the use of these shapes to create new types of immersed wave breakers  
137 could reduce the current speed behind the structure without reflecting the energy to  
138 the sides of the structure. In this case, wave breakers should not increase erosion of  
139 non-protected areas.

140 This work aims to find new bio-inspired wave breaker shapes that could optimize the  
141 erosion reduction behind the structure without eroding nonprotected areas in order to  
142 be a solution to control coastal erosion. It is meant to be a proof of concept and  
143 therefore start to quantify the interaction of these shapes and the swell. The location  
144 has been taken as an example but the simulation data are not focused on one precise  
145 location because the aim was not to study in detail one particular case. Wave-breakers  
146 were 3D modeled in a submerged environment representing the Bay of Biscay area  
147 and their impact on waves was studied by numerical simulation. Two bio-inspired forms  
148 of wave-breakers were modeled based on the nest of *Torquigener albomaculosus* and  
149 the root system of mangroves. These models were compared by numerical simulation  
150 with usual wave-breakers. First, the modelling of the wavebreakers will be detailed in  
151 this paper, then the results of the different numerical simulations, carried out with a  
152 CFD tool as well as a Python program, will be explained in order to discuss the interest  
153 of biomimicry for the protection against coastal erosion.2. Material and Method

154

## 155 2.1. Model development

156 In this study, a three-dimensional Computational Fluid Dynamics (CFD) software has  
157 been used to calculate the effects of bio-wave breakers on sea currents and on swell.  
158 It is based on the Lattice-Boltzmann Method (LBM). Simulations were made with a  
159 free-surface model. It means that the fluid is in the lower part of the simulation and is  
160 the only element considered (Fig. 1). The software resolves the Navier-Stokes and the  
161 Boltzmann equations ([Dassault Systèmes, 2021](#)). The Navier-Stokes equations are  
162 expressing the conservations of mass (Eq.1), of the momentum (Eq.2) and of the  
163 energy (Eq.3). These are partial differential equations ([Jamshed, 2015](#)).

$$164 \quad \delta\rho/\delta t + \nabla \cdot (\rho \vec{V}) = 0 \quad : \quad Eq.1$$

165

166 
$$\delta(\rho\vec{V})/\delta t + \nabla \cdot (\rho\vec{V}\vec{V}) = -\nabla p + \nabla \cdot \Sigma + \rho\vec{g} \quad : \text{Eq.2}$$

167

168 
$$\delta(\rho E)/\delta t + \nabla \cdot (\rho E\vec{V}) = -\nabla \cdot (P \cdot \vec{V}) + \rho\vec{g} \cdot \vec{V} + \nabla \cdot \vec{q} + \nabla \cdot \vec{q}_R \quad : \text{Eq.3}$$

169

170 With  $\rho$  the density,  $t$  the time,  $V$  the eulerian speed,  $\nabla$  the divergence,  $\Sigma$  the stress  
 171 tensor,  $g$  the external mass-forces,  $E$  the total energy per mass unit,  $q$  the heat flow of  
 172 the thermal conductivity, and  $q_R$  the heat flow of the radiation.

173 
$$f_\alpha(x + c_\alpha \delta x, t + \delta t) = f_\alpha(x, t) - 1/\tau * [f_\alpha(x, t) - f_\alpha^{eq}(x, t)] \quad : \text{Eq.4}$$

174 With  $f_\alpha$  the particle distribution function in direction,  $x$  the lattice node  $c_\alpha$  the particle  
 175 discrete vectors,  $t$  the discrete times,  $\delta t$  the constant time step,  $\tau$  the relaxation time  
 176 due to the fluid viscosity and  $f^{eq}$  the collision operator obtain with an order 2 Taylor  
 177 development of the Maxwell-Boltzmann distribution function.

178 The Boltzmann equation (Eq.4) is a distribution function of each group of particles. This  
 179 model assumes that the diffusion, or the motion of particles, is equal to the collision  
 180 ([Heubes et al., 2013](#)). LBM is a meshless particle-based method. The approach is  
 181 completely Lagrangian. It is one of the most powerful methods to calculate the  
 182 interaction between complex geometries and turbulent fluids ([Satjaritanun et al., 2018](#)).  
 183 It doesn't need to have a Sliding Mesh and a Multiple Reference Frame. The simulation  
 184 generates a Lattice element and organizes it in an Octree structure. It considers both  
 185 micro and mesoscopic processes in order to obtain correct macroscopic equations.  
 186 The LBM calculates a statistical distribution function with the variables, while  
 187 conserving mass, momentum, and energy (Eq. 1-3) ([Chen and Doolen, 1998](#)).

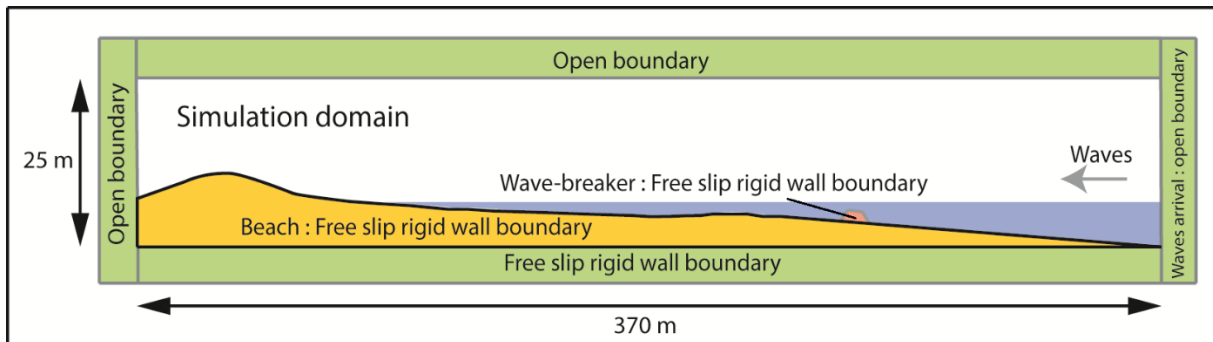
188 It uses a Wall-Modeled Large Eddy Simulation (WMLES) model. The hypothesis is  
 189 done that smaller turbulences are instantly and completely dissipating all the energy  
 190 they receive from the greater scale's structures ([Grondeau et al., 2016](#)). This increases  
 191 the efficiency by reducing the meshing operation and also the computational time  
 192 ([Satjaritanun et al., 2018](#)). The wall function used by the software to model the  
 193 boundaries is a unified non-equilibrium wall function. It means that the average velocity  
 194 is sensitized to the effects of the pressure gradient. It also uses the concept of two-  
 195 layer-based to compute the sum of the kinetic energy of the turbulences ([Dassault  
 196 Systèmes, 2021](#)). The software chosen for the simulations was Xflow®2000, a  
 197 commercial LBM CFD solver.

198

199 In all the simulations, the values of some parameters have been kept. A 3D free-  
 200 surface isothermal environment was used. The temperature variation was considered  
 201 to be nil, therefore negligible even if it is not the case in the reality. The aim was to  
 202 understand the interaction between the wave breakers shapes and a common swell.  
 203 The gravity of the fluid was at  $9.81 \text{ m.s}^{-2}$ . This is due to the orientation of the spatial  
 204 axes during the numerical simulation. The z-axis representing the altitude is usually  
 205 oriented upwards, so gravity has a negative sign. The dimensions of the domain were

206 defined: 370 m long, 25 m high, and 350 m large (Fig. 1). All the water channel  
 207 boundaries were open except for the ground that was a free-slip rigid wall boundary.  
 208 The beach and the wave breakers were considered as free-slip rigid wall boundaries  
 209 too (Fig. 1). The mesh was 0.25 m large around the wave breakers and 1 m large  
 210 everywhere else. This size was conditioned by the software and by the computer. If  
 211 the mesh size was smaller, the software couldn't generate the Lattice domain. The fluid  
 212 was seawater with a temperature of 20°C and a density of 1024 kg.m<sup>-3</sup> (Vandermeirsch  
 213 *et al.*, 2012).

214 Fig.1 (Small column size)

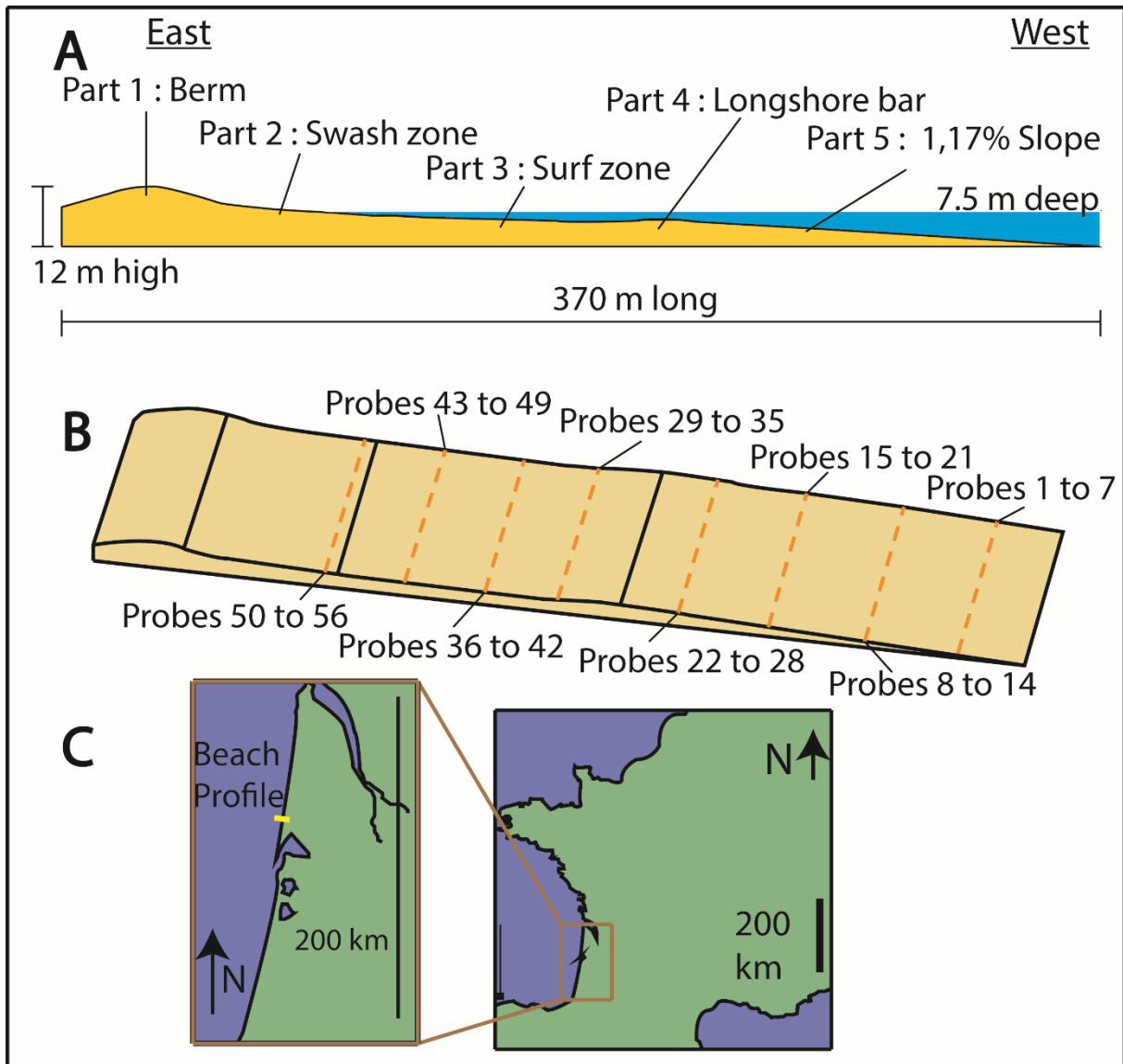


215  
 216 2.2. Parameters of the simulation

217 For this study, the action of wave breakers was simulated in the Bay of Biscay in  
 218 France. According to Migniot and Lorin (1979), the swell is more powerful in the Atlantic  
 219 than in the Mediterranean Sea, therefore selecting the Atlantic Ocean as a study area  
 220 is interesting for the quantification of the maximum effect of the swell. The goal was to  
 221 simulate a similar morphology as the beach on the coast, near Biscarrosse (France) (  
 222 44° 21' 3.55" N 1° 9' 58.424" W). In order to achieve it, the bathymetric data from  
 223 January 2021 of the European Marine Observation and Data Network (EMODnet) has  
 224 been used to design the beach profile with CatiaR2021X® (Fig.2 A, B). The beach  
 225 profile was inspired by these data and extrapolated to get a 350 m large structure. This  
 226 could not be considered as a realistic beach but the goal of this study is limited to  
 227 understand the interaction between the wave breakers and the swell. The longshore  
 228 bar was considered as fixed in this study because the simulation duration was of 45 s.  
 229 For each simulation and each wave breaker, the depth at the top of the wave breaker  
 230 was 1.5 m and the mean distance with the coast was the same. A study considering  
 231 shape complexity and mechanical characteristics of each wave breaker could be  
 232 interesting but is out of scope for this work.

233

234 Fig.2 (Small column size)



235

236 As explain in Brivois et al., in 2012,"The Aquitanian Coast (SW France) is an  
 237 approximately 250 km long straight low coast bordered by high aeolian dunes".  
 238 Prederos et al (1996) describes the sediments of the study area as medium to fine  
 239 sands with a grain size ranging from 200 to 400  $\mu$ m. According to Wright and Short  
 240 1984 classification, the majority of Aquitaine beaches are intermediate beaches with  
 241 Transverse Bar and Rip (TBR), or low tide bar/rip as defined by Masselink and Short  
 242 (1993).During spring tides, in the study area, the sea level rises from 0.3 m to 5 m  
 243 (Butel et al., 2002), classifying these beaches as mesotidal.

244 As explained by Castelle and Bonneton in 2002, tidal currents are largely negligible  
 245 compared to those induced by the swell. However, they were calculated by Sénéchal  
 246 et al., in 2009 and have a speed of 0.2 m.s<sup>-1</sup> from West to East during the flood and  
 247 from East to West during the ebb.

248 The wave regime has a mean annual significant wave height of 1.36 m and a mean  
 249 period of about 8 s with a strong seasonal dependence linked to the NAO (Butel et al.  
 250 2002; Dupuis et al., 2006; Sénéchal et al., 2009; Carles et al., 2011; Le Cozannet et  
 251 al., 2011 et al. 2009, Brivois et al., 2012).

252 [Brivois et al., \(2012\)](#) describe the wave conditions as evolving from low energy waves  
 253 during the summer oriented NW to very high energy waves during winter storms  
 254 generating west to NW swells.

255 Regarding the wave breakers characteristics, several studies cover the optimum  
 256 parameters ([Carpentier and Brosselard-Faidherbe, 1986](#); [Delage, 1954](#); [Massel and](#)  
 257 [Gourlay, 2000](#); [Toyoshima et al., 1966](#)). For example, the efficiency of a structure is  
 258 linked to its depth and its distance to the coast ([Delage, 1954](#)). These parameters are  
 259  $D$  the distance between the wave breaker and the coast,  $L$  the length of the structure,  
 260  $H$  its height,  $p$  the depth where the wave breaker is located,  $\lambda$  the swell wavelength,  
 261 and  $T$  the wave period.

262

263 Table 1

Parameter	Value	References
$D$	225 m	<a href="#">Massel and Gourlay, 2000</a>
$L$	285 m	<a href="#">Toyoshima et al., 1966</a>
$H$	3.55 m	<a href="#">Delage, 1954</a>
$p$	4 m	Found in the simulation
$\lambda$	102 m	<a href="#">Carpentier and Brosselard-Faidherbe, 1986</a>
$T$	8.0 s	<a href="#">Carpentier and Brosselard-Faidherbe, 1986</a>

264

### 265 2.3. Existing wave breakers

266 The first wave breakers modeled were inspired by existing shapes like trapezoidal or  
 267 elongated tubes. Both shapes were found in the literature. Trapezoidal shape for  
 268 immersed wave breaker is common in mathematical articles, bench tests, and real  
 269 beach analyses ([Hornack, 2011](#); [Repousis et al., 2014](#)). Authors assume that other  
 270 types of existing wave breakers could be used, but the main goal of this study was only  
 271 to suggest new bio-inspired shapes for wave breakers and not to make an exhaustive  
 272 study on wave breakers. This geometrical shape is easier to create and to settle on  
 273 the seafloor than more complex shapes. Elongated tubes are another wave breaking  
 274 shape which is induced by the process of creation of the wave-breaker. They are  
 275 Multipurpose Artificial Reefs (MPAR) and are used to generate a surfable wave break  
 276 type as well as reducing the swell energy. A geotextile tube is set up, then filled with  
 277 sand before being settled down on the seafloor. It is easier and cheaper to install than  
 278 concrete, and its shape is more continuous and regular than a rockfill. They could be  
 279 damaged by a rupture of the geotextile. This shape has been studied by different  
 280 studies with Computational Fluid Dynamics and beach studies ([Hedge, 2010](#); [Isebe et](#)  
 281 [al, 2008](#)). Both shapes have been modeled on the 3DEXPERIENCE Platform with  
 282 CatiaR2021X®.

283

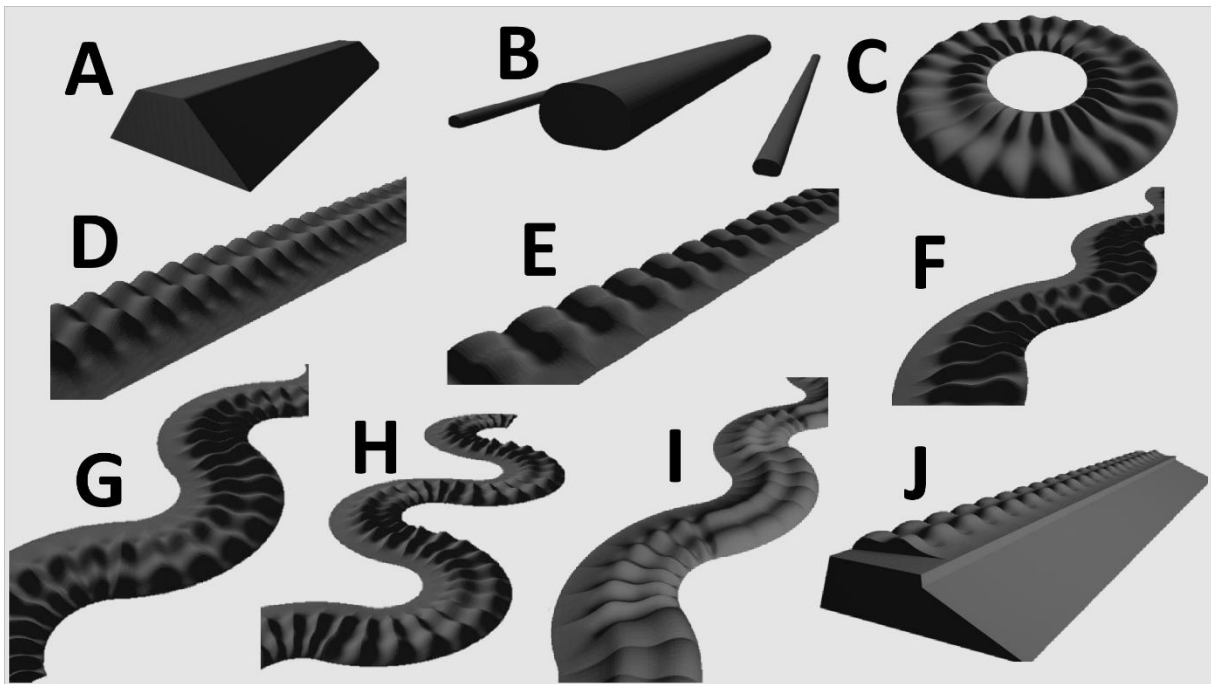
## 284 2.4. Bio-inspired wave breakers

285 The first inspiration for designing bio-inspired wave breakers was the *Torquigener*  
286 *albomaculosus*' nest. This fish was observed in the Pacific Ocean, near the Japanese  
287 coast (Kawase *et al.*, 2013). Different nests have been found between 10 and 30  
288 meters deep. The 10 cm fish takes less than 10 days to create a circular 2 meters large  
289 shape in the sand. It is composed of two concentric parts (Fig.3 C). The outer ring with  
290 24 to 28 cm high peaks, 12 cm apart from each other. The inner circle is a small  
291 depression with an irregular pattern (Kawase *et al.*, 2017). All the nests have usually  
292 the same outer ring. There is on the outside part a bigger dune and on the inside part  
293 a smaller one. This nest is exposed to currents going between 0.8 and 1.0 m.s<sup>-1</sup>. The  
294 nest could cause a slowdown of the current because of its particular geometrical  
295 pattern. This current could be broken by the greater ripple and then be uniformed in  
296 the centre of the nest by the smaller one (Kawase *et al.*, 2013; Kawase *et al.*, 2017;  
297 Matsuura., 2015).

298 The nest has been modelized on the 3DEXPERIENCE Platform with CatiaR2021X®.  
299 2D sketches and multi-section solids were used to create a part of the nest. Then, it  
300 was duplicated 24 times to get a 3D model of the entire nest (Fig.3 C). Following this  
301 step, different types of wave-breaker were modelized. In order to do so, models of  
302 existing shapes as a trapeze and three elongated tubes were done (Fig.3 A, B).  
303 Following this logical path, shapes inspired by the nest were created. Each model  
304 added another characteristic of the nest. The first one (Fig.3 D) was straight and kept  
305 the order of the two ripples; the taller one before. The second one (Fig.3 E) was still  
306 straight but put an angle between every two dunes. The third one (Fig.3 F) added the  
307 circular pattern by being built with quarters of the nest. The fourth one (Fig.3 G) took  
308 larger parts of the nest; it was made with thirds of the nest. The fifth one (Fig.3 H)  
309 continued this logic with halves of the nest. The sixth one (Fig.3 I) took quarters of the  
310 nest but the taller dunes were always facing the sea. From the third to the sixth, wave  
311 breakers had a sinusoidal shape. The last one (Fig.3 J) was the merge of two shapes.  
312 The base was a trapeze-shaped wave-breaker and the top was a straight bio-inspired  
313 shape (Fig.3 D) All these shapes were rescaled to have the same height and the same  
314 length given in table 1.

315

316 Fig.3 (Small column size)



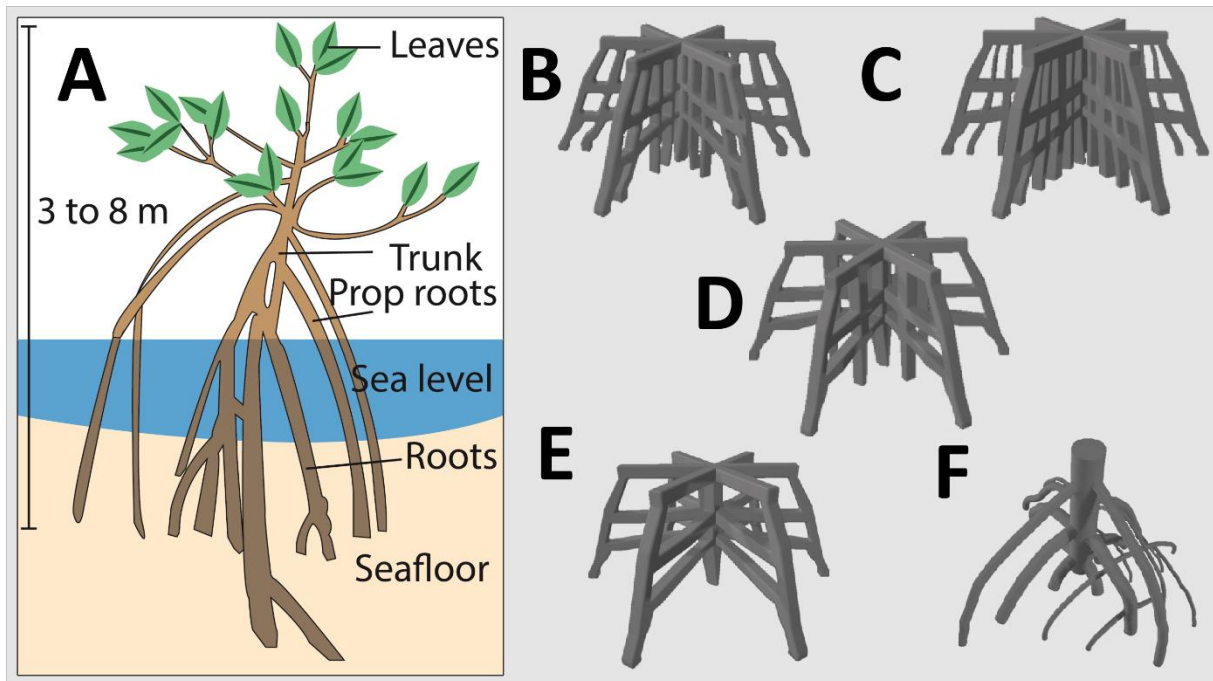
317

318 The second inspiration was the mangroves. [Horstman et al. \(2014\)](#) described  
 319 mangroves as an ecosystem located on subtropical tidal coasts. They are composed  
 320 of trees and shrubs from distinct species which are exposed to waves and flooding.  
 321 They form, with a coral reef generally, a buffer between land and sea, contributing to  
 322 wave attenuation ([Horstman et al., 2014](#); [Hong Phuoc and Massel, 2006](#)) and  
 323 consequently, helping in coastal stabilization([Anthony, 2004](#); [Van Santen et al., 2007](#)).  
 324 Thereby, the question is, can mangrove-inspired wave breakers be effective in  
 325 reducing coastal erosion? Mangroves are constituted of varied species of plants that  
 326 interact differently with the swell and can be more or less effective to protect the  
 327 coastline ([Hong Phuoc and Massel, 2006](#)). One of the species with the highest wave  
 328 height reduction is the *Rhizophora* (Fig.4 A) ([Phan et al., 2014](#); [Lee et al., 2021](#)).

329 In order to test the capacity of mangroves to act as wave breakers, 3D models have  
 330 been created on the 3DEXPERIENCE Platform with CatiaR2021X. Two main types of  
 331 models have been tested, following a symmetric geometry or a chaotic geometry. The  
 332 symmetric geometry had three axes separated by an angle of 60° with a radius of 7.78  
 333 meters and a height of 3.55 meters. Different roots' densities have been tested with 3,  
 334 5, 8 and 10 vertical roots per axis (respectively Fig.4 E,D,C,B). The chaotic structure  
 335 followed a semi-sphere geometry with a radius of 3.71 meters and a height of 3.55  
 336 meters (Fig.4 F). The tools used most of the time on CatiaR2021X to create these  
 337 models were the extrusion, used to create the principal structure, and the ridge, used  
 338 to create the branch attached to the main structure. Each model has been duplicated  
 339 to build rows to form wave breakers. There are a 15m distance between each centre  
 340 of mangrove so that there are 0.5 m of gap between two shapes. The aim of testing  
 341 these shapes is not to study the technical properties of the wave breakers but to reveal  
 342 if their interaction with the swell can reduce the energy of the seafloor currents. For the  
 343 same reason, the material used to create these shapes is not considered.

344

345 Fig.4 (Small column size)



346

### 347 2.5 Agents defining erosion

348

349 [Hjulström \(1935\)](#) defined grain size and current velocity as important factors in  
350 sedimentary movement. Subsequently, in the 1970s, sediment transport modelling  
351 was initiated, resulting in the development of several formulae that describe longshore  
352 drift - a critical aspect of sedimentary stock movements - and lead to erosion. These  
353 formulae were proposed by [Longuet-Higgins \(1970\)](#), [Komar and Inman \(1970\)](#), [Komar](#)  
354 [\(1979\)](#), and [Cerc \(1984\)](#).

355

356 Whether it is a reflective or diffractive shoreline, as defined by [Masselink and Short](#)  
357 [\(1993\)](#), sedimentary transport important factors are: i) morphology (beach barred or  
358 unbarred), ii) slope (beach and nearshore slope), iii) grain size, iv) wave height and  
359 angle and v) currents. With the tidal current's exception, the currents are derived from  
360 the height and angle of the swell (drift current, swash and backwash current). To limit  
361 erosion, it is necessary to reduce: the wave height and/or the wave angle and/or the  
362 currents.

363

364 The model's input parameters are: i) granulometry (between 0.10 and 0.20 mm) and  
365 ii) bottom currents defined by [Migniot and Lorin study in 1979](#) (1.4 m/s maximum). The  
366 grain size is not simulated. It is used in this study to interpret simulation results. For a  
367 particle size between 0.10 and 0.20 mm, a current of 1.0 to 5.0 cm/s speed will  
368 transport the particles (suspension, creep and saltation) with a 20 cm/s speed. The  
369 simulations objectives are: i) to observe and understand the interaction between  
370 currents/swells and new forms of bio-inspired wave breakers, and ii) to observe, if  
371 possible, the variations of current speed with the implementation of wave breakers.  
372 The drift current will not be considered in these simulations, nor the wave height due  
373 to computational cells size.

374

## 375 2.6. Location of the observation points

376 A simulation with all the characteristics identified above has been created. 56  
377 observation points (or probes) were located as eight lines of seven on the seafloor.  
378 They are fixed points that identify the nearest cell to their locations and write out the  
379 cell values with a certain frequency. For example, in the simulations, each point  
380 recorded the value of the speed every 0.00345 seconds (290 Hz). The four first lines  
381 (points 1 to 28) are placed on a gentle slope from the entrance of the simulation to the  
382 edge of the longshore bar, a submarine dune (Fig.2). The fifth line (point 29 to 35) was  
383 just behind this bar. The sixth one (points 36 to 42) is in the surf zone. Finally, the two  
384 last lines (points 42 to 56) are on the floor of the swash zone (Fig.2).

385 Then, two situations were studied: at ebb tide and flood tide. These were the control  
386 simulations. Each observation point gave more than 13,000 speed values for each  
387 simulation. Then the simulation was kept the same as were implemented the wave  
388 breakers, one at a time. For every shape, two simulations for both tide were done. In  
389 addition, the Python program was used to compare these simulations with their  
390 controls. With this method, it was possible to characterize the efficiency of the wave-  
391 breaker to slow down the current and consequently the swell erosion.

392

## 393 3. Results

394

### 395 3.1. Control simulations

396 The first thing to do was the control simulations. There were two with the average swell  
397 at both tides. When the depth is lower than one and a half time the height of the wave,  
398 the wave collapses. This always happened just before the longshore bar (Fig.2). After  
399 this, the sea seemed smoother but the current was still observed with a maximum  
400 average speed of  $1.38 \text{ m.s}^{-1}$  on the seafloor. This would be enough to move sand  
401 particles easily. The fastest currents seemed to stay at the top of the water. This was  
402 a good thing because waves were already broken by the longshore bar and there was  
403 still particle displacement, which implied positioning the wave breakers upstream of  
404 the bar so that the waves collapsed earlier.

405 Regarding the seafloor current speeds, at flood tide, the speeds were between 0.55  
406 and  $0.45 \text{ m.s}^{-1}$  at the three first points lines. The current accelerated around the  
407 longshore bar with  $0.7 \text{ m.s}^{-1}$  on the fourth line and  $0.85 \text{ m.s}^{-1}$  on the fifth line. Then, the  
408 seafloor current slowed with a  $0.80 \text{ m.s}^{-1}$  speed at the sixth line and a  $0.62 \text{ m.s}^{-1}$  speed  
409 at the seventh line. The sea level reached sometimes the eighth line but it registered  
410 an average speed of  $0.05 \text{ m.s}^{-1}$ . The average speed of all points was  $0.52 \text{ m.s}^{-1}$ .

411 At ebb tide, the speed decreased on the first three lines from  $0.46 \text{ m.s}^{-1}$  to  $0.26 \text{ m.s}^{-1}$ .  
412 Then, the current accelerated to reach  $0.50 \text{ m.s}^{-1}$  on the fourth line and  $0.72 \text{ m.s}^{-1}$  right  
413 behind the longshore bar, on the fifth line. At the sixth line, the maximum seafloor  
414 current speed was reached with  $1.38 \text{ m.s}^{-1}$ . Then, the speed decreased to  $0.76 \text{ m.s}^{-1}$   
415 on the seventh line. The sea level didn't reach the last line so that the last points didn't  
416 register any value. The average value for all the points was  $0.63 \text{ m.s}^{-1}$ .

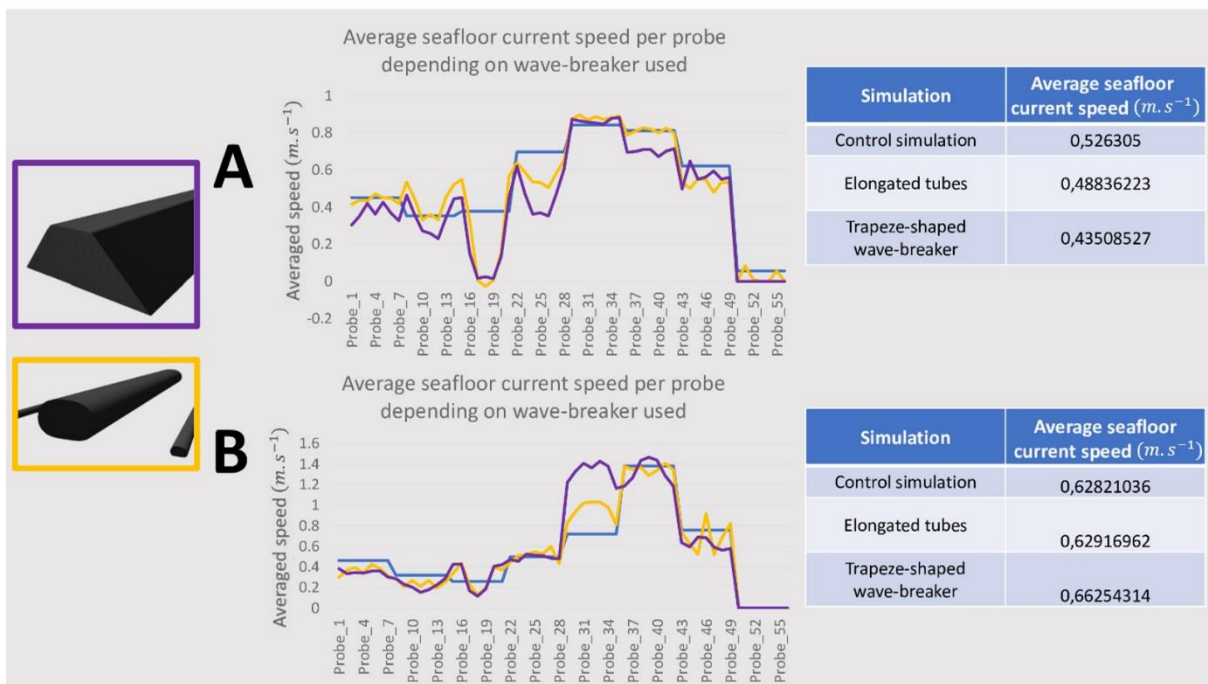
417

### 418 3.2. Existing wave breakers

419 The second step was the simulation of both existing models with the average swell.  
 420 The depth of the top of the structure was 1.5m. The wave breakers had a similar  
 421 behaviour (Fig.5). At flood tide, there was on the third line of points a slowdown  
 422 between -0.4 and -0.35  $m.s^{-2}$  that kept the speed near  $0.0 m.s^{-1}$ . The negative  
 423 acceleration means a mean reduction in the acceleration of the current measured at  
 424 the observation points. The fourth observation point line showed the same changes  
 425 but with smaller intensity. From probes line n°5 to n°7 (probes 29 to 49 represented in  
 426 Fig.5), there were no major changes between the control and the simulations. The last  
 427 line showed that the sea level had not reached all the observation points. At ebb tide,  
 428 the behaviour of the current was completely different. The biggest slowdown in both  
 429 cases was  $-0.2 m.s^{-2}$  and some accelerations were over  $+0.3 m.s^{-2}$  for the elongated  
 430 tube and  $+0.7 m.s^{-2}$  for the trapeze. These maximum accelerations were located on  
 431 the fifth line, right after the longshore bar. The average change was  $-0.091 m.s^{-2}$  at  
 432 flood tide and  $+0.034 m.s^{-2}$  at ebb tide with the trapeze. With the elongated tubes, it is  
 433  $-0.038 m.s^{-2}$  at flood tide and  $+0.001 m.s^{-2}$  at ebb tide.

434

435 Fig.5. (Full page width)



436

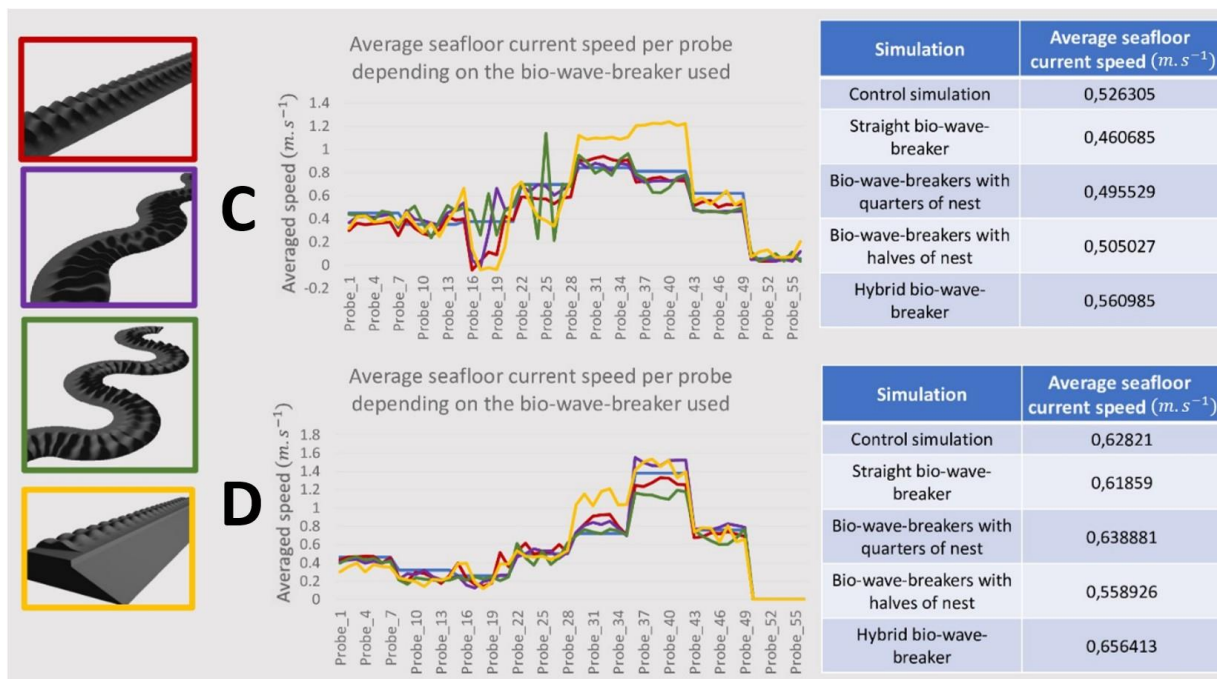
### 437 3.3. Nest-inspired wave breakers

438 The third step was the simulation of the nest-inspired wave breakers with the average  
 439 swell. Both straight wave-breaker created little accelerations (e.g.  $+0.1 m.s^{-2}$ ) and a  
 440 general slowdown at flood tide. These results changed drastically at ebb tide. There  
 441 were some accelerations of  $+0.25 m.s^{-2}$  around the third line (just behind the structure)  
 442 and around  $+0.15 m.s^{-2}$  next to the fourth and fifth line, around the longshore bar. The  
 443 four sinusoidal wave-breaker had different results. They all presented some zones with

444 accelerations (e.g.  $+0.4 \text{ m}\cdot\text{s}^{-2}$  for the shape with thirds of nest at flood tide) and other  
 445 areas with slowdowns (e.g.  $-0.19 \text{ m}\cdot\text{s}^{-2}$  on the same model at ebb tide). The location  
 446 of these zones and the values were depending on the shape and the tide. None of  
 447 them showed a general slowdown at both tides. The last simulation with the nest shape  
 448 was the one with the hybrid wave-breaker (J on Fig.3). It was the only shape that  
 449 generated a general acceleration at the fifth and sixth observation point lines, right  
 450 behind the longshore bar. The average speed value was  $0.56 \text{ m}\cdot\text{s}^{-1}$  with the wave-  
 451 breaker and  $0.53 \text{ m}\cdot\text{s}^{-1}$  without it. At ebb tide, there were still consequent acceleration  
 452 zones (e.g.  $+0.5 \text{ m}\cdot\text{s}^{-2}$ ) but no more important slowdown areas (Fig.6). The average  
 453 speed ( $0.66 \text{ m}\cdot\text{s}^{-1}$ ) was superior to the control average value ( $0.63 \text{ m}\cdot\text{s}^{-1}$ ). To sum up,  
 454 no model, with these parameters, generated a global slowdown of the current on the  
 455 seafloor.

456

457 Fig.6. (Full page width)



458

### 459 3.4. Mangrove-inspired wave breakers

460 The fourth step was the simulation of the mangrove-inspired wave breakers with an  
 461 average swell. On the first hand, simulations with two rows of a symmetrical model  
 462 have been done (Fig.4 B). At flood tide, only four observation points showed an  
 463 acceleration over  $+0.1 \text{ m}\cdot\text{s}^{-2}$ . They were all on the sides of the second and third points  
 464 lines, just next to the structure. Seven points showed a slowing of  $-0.5 \text{ m}\cdot\text{s}^{-2}$ . The  
 465 average seafloor speed changed from  $0.53 \text{ m}\cdot\text{s}^{-1}$  in the control to  $0.44 \text{ m}\cdot\text{s}^{-1}$  in this  
 466 case. At ebb tide, the maximal acceleration was around  $+0.2 \text{ m}\cdot\text{s}^{-2}$  at point 32, just  
 467 behind the longshore bar. 42 points showed a slowdown and the average speed  
 468 changed from  $0.63 \text{ m}\cdot\text{s}^{-1}$  in the control to  $0.55 \text{ m}\cdot\text{s}^{-1}$ .

469 On the second hand, simulations with two rows of a chaotical model have been done.  
 470 At flood tide, the first four observation points lines showed an acceleration. Five points

471 had a change over  $+0.1 \text{ m.s}^{-2}$  and two were over  $+0.2 \text{ m.s}^{-2}$ . The four last lines put in  
472 evidence a slowdown that reached  $-0.54 \text{ m.s}^{-2}$  at the seventh line. The average  
473 seafloor speed changed from  $0.53 \text{ m.s}^{-1}$  in the control to  $0.42 \text{ m.s}^{-1}$  in this case. At ebb  
474 tide, only the seven points of the fifth line were showing an acceleration. This maximum  
475 value was at  $+0.08 \text{ m.s}^{-2}$  and the biggest slowdown was at  $-0.73 \text{ m.s}^{-2}$  at point 37, on  
476 the sixth line. The average speed changed from  $0.63 \text{ m.s}^{-1}$  in the control to  $0.44 \text{ m.s}^{-1}$ .

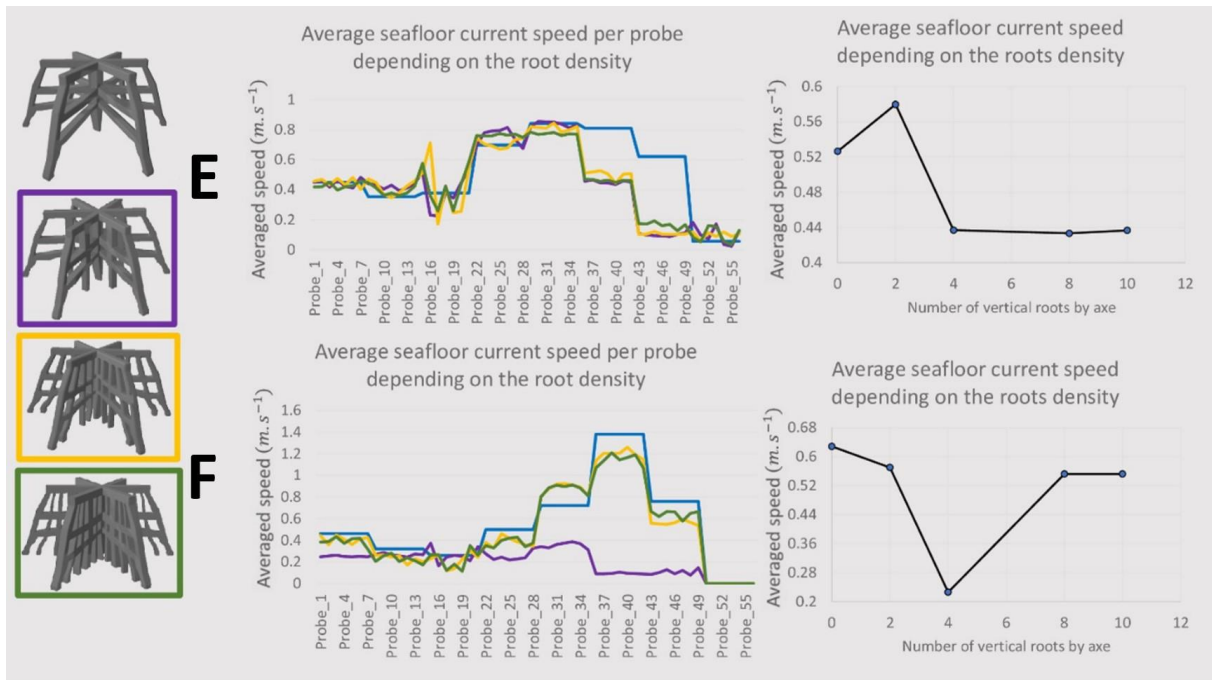
477

478 Then, several roots' densities have been tried to determine if there was a link between  
479 density and efficiency. At flood tide, the simulation with two vertical roots per axis  
480 showed accelerations at the centre of each observation point line. The average speed  
481 was higher than the control simulation with a value of  $0.58 \text{ m.s}^{-1}$ . The other simulations,  
482 with four, eight and ten roots per axis, showed more or less the same behaviour. The  
483 first four lines showed an acceleration. Two points had a change over  $+0.1 \text{ m.s}^{-2}$  and  
484 were at  $+0.2 \text{ m.s}^{-2}$ . The three following lines put in evidence a slowdown that reached  
485  $-0.50 \text{ m.s}^{-2}$  at the seventh line. The eighth line showed an acceleration between  $+0.1$   
486 and  $+0.0 \text{ m.s}^{-2}$ . The average speed was at  $0.53 \text{ m.s}^{-1}$  in the control and  $0.44 \text{ m.s}^{-1}$  in  
487 all the simulations.

488 At ebb tide, on the one hand, the behaviour was the same with 2, 8 or 10 roots per  
489 axis. The average speed was around  $0.55 \text{ m.s}^{-1}$  with a control at  $0.63 \text{ m.s}^{-1}$ . There  
490 were less than ten observation points that showed a non-zero acceleration with only  
491 five observation points over  $+0.1 \text{ m.s}^{-2}$ . Only the fifth observation line, just behind the  
492 longshore bar put in evidence a general acceleration. The other points registered a  
493 slowdown between  $-0.05$  and  $-0.31 \text{ m.s}^{-2}$ . On the other hand, with 4 roots on each axis,  
494 the behaviour was completely different. There were only two points with accelerations  
495 of  $0.11$  and  $0.08 \text{ m.s}^{-2}$ . Moreover, the sixth line showed a slowdown around  $-1.3 \text{ m.s}^{-2}$   
496 (Fig.10 B). The average speed was around  $0.22 \text{ m.s}^{-1}$ . One important thing was that  
497 the maximum speed was at  $0.38 \text{ m.s}^{-1}$  when it was  $1.4 \text{ m.s}^{-1}$  in the control (Fig.7 B).

498

499 Fig.7. (Full page width)



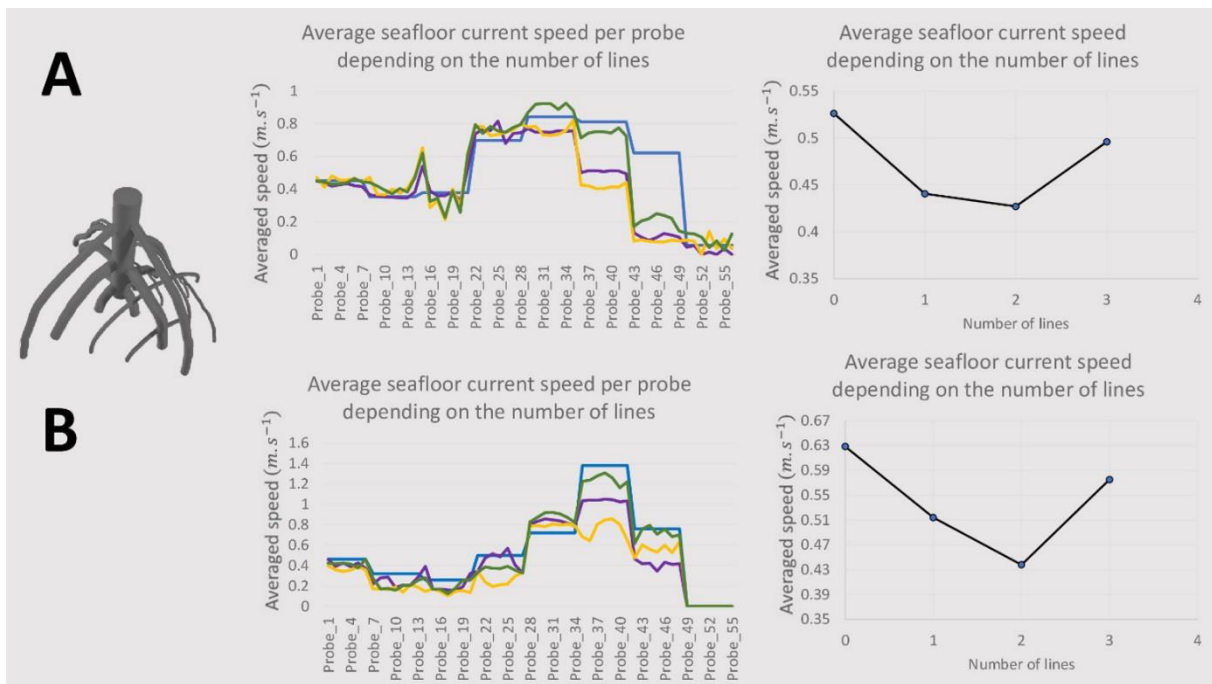
500

501 For the fifth step, different numbers of consecutive lines of the chaotical model have  
 502 been tested to determine if there was a link between this parameter and the efficiency  
 503 of the wave breaker. Each line's centre was about 15 m apart, which resulted in a gap  
 504 between lines of 0.5 m. This is a gap similar to the one between each mangrove in the  
 505 line. At flood tide, the general behaviour was the same but the values were changing  
 506 depending on the number of lines. There were a few accelerations over + 0.1 m.s<sup>-1</sup> and  
 507 one over +0.2 m.s<sup>-2</sup> at point 14. On the fifth line of points, the only simulation to show  
 508 an acceleration was the one with three rows of mangroves. The simulation with two  
 509 rows registered the lowest or second-lowest seafloor current speed at every point  
 510 except at points 14, 23, 53 and 55. The average speed was at 0.44 m.s<sup>-1</sup> with one row,  
 511 at 0.43 m.s<sup>-1</sup> with two rows and 0.49 m.s<sup>-1</sup> with three rows (Fig.8 A).

512 At ebb tide, the general behaviour was still the same between the three simulations  
 513 but the values were changing depending on the number of rows. Only a few points  
 514 registered an acceleration but on the fifth line of observation points, there was an  
 515 acceleration that could go up to + 0.2 m.s<sup>-1</sup> when there were three mangroves' rows.  
 516 In general, the average seafloor current speed with two rows of mangroves was the  
 517 lowest. The only exception was between points 42 and 48, where the lowest value was  
 518 in the one-row case. The average speed was at 0.63 m.s<sup>-1</sup> in the control, at 0.51 m.s<sup>-1</sup>  
 519 with one row, at 0.44 m.s<sup>-1</sup> with two rows and at 0.58 m.s<sup>-1</sup> with three rows (Fig.8 B).

520

521 Fig.8. (Full page width)



522

523 Finally, different current orientations were tested on the most efficient mangrove-  
 524 inspired wave breakers. The goal is to observe if different current orientations will  
 525 change the impact of the wave breakers on erosion. For this purpose four different  
 526 orientations were tested for the flood tide. An angle of 30, 45, 60 and 75 degrees to  
 527 the normal flow was chosen. A control simulation was run for each of these angles to  
 528 compare the results. The average velocity of the control simulation and the breaker  
 529 simulation is shown in Table 2

530

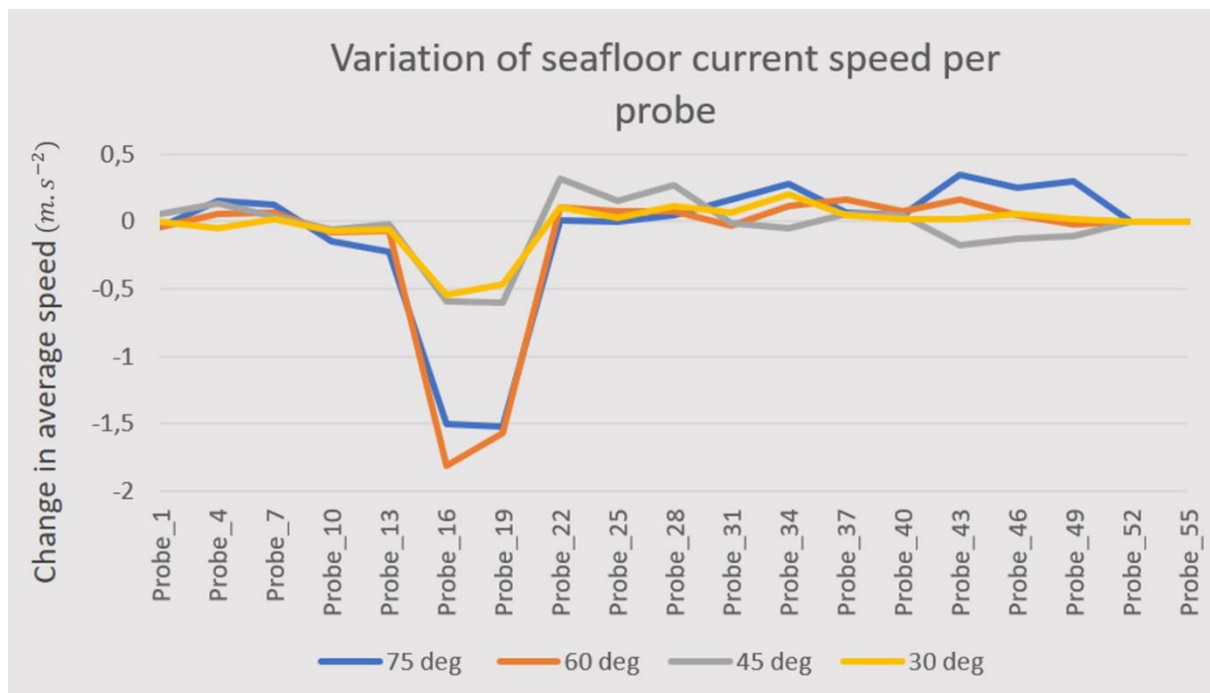
531 Table 2

Flow angle	75°		60°		45°		30°		0	
Simulation	Control	Wave-Breakers								
Mean Velocity ( $m \cdot s^{-1}$ )	0,83	0,74	1,05	0,94	0,58	0,56	0,57	0,54	0,52	0,43

532

533 The simulations performed with an angle will result in an increase of the water velocity  
 534 at the ground level. The behaviour of the water deceleration is different for the  
 535 simulation with orthogonal current than for the simulations with an angle of current. But  
 536 this behaviour is similar between the different simulations with a current angle. The  
 537 majority of the deceleration is located on the third line (Fig.9), ranging from a  
 538 deceleration of 1.8  $m \cdot s^{-1}$  for the 60° simulation to 0.55  $m \cdot s^{-1}$  for the 30° simulation.  
 539 From the 4th to the 5th line an increase of the speed oscillates between 0 and 0.4  $m \cdot s^{-1}$ .  
 540 For the current at 45° a decrease in velocity from 0.24 to 0.13  $m \cdot s^{-1}$  for the 6th and  
 541 7th line appeared. Whereas the simulation at 75° leads to an increase in velocity from  
 542 0.35 to 0.25  $m \cdot s^{-1}$

543 Fig.9. (Full page width)



544

545 3.5 Validation of numerical simulations

546

547 The experimental data needed to validate the simulations was found in the scientific  
 548 literature. The results of the control simulations and simulation with existing wave  
 549 breakers have been compared with experimental data. If it validated the first  
 550 simulations, it would make the other simulations with new types of submerged wave  
 551 breakers more credible.

552 Firstly, the results of the control simulations have been compared to check the validity  
 553 of the interaction between the beach and the wave function. The main criteria to  
 554 compare natural waves and simulated waves were the breaking phase and location.  
 555 According to [Larson and Kraus \(1992\)](#), the waves breaking zone is located around the  
 556 longshore bar when there is one. [Migniot and Lorin \(1979\)](#) explain this with the fact  
 557 that the waves tend to collapse when the water depth is smaller than 1.5 times the  
 558 wave crest height. This behavior was present in the simulations. The waves collapsed  
 559 just before the longshore bar (Fig. 2). At this location, the slope made the depth lower  
 560 than 3 meters and the wave crests were 2 meters high. It was natural that waves broke  
 561 at this location.

562 Secondly, the interaction between the fluid and existing wave breakers has been  
 563 compared with experimental data. The first point that was common in most papers is  
 564 that the wave-breaker slows the current right behind it ([Balouin et al., 2016](#); [Boulet et al., 2018](#);  
 565 [Rasidah et al., 2010](#); [Williams et al., 2018](#)). At flood tide, this behavior was  
 566 observed with both existing wave breakers (Fig. 5A) (points 16-19 and points 23-26).  
 567 The slowdown was maximum just behind the center of the structure (points 16-19).  
 568 According to [Balouin et al. \(2016\)](#), the submerged wave-breaker protects the coastline  
 569 behind it but tends to parallelize the shoreline to the structure by eroding the changes

570 in the shoreline direction. [Balouin et al. \(2016\)](#) explain it by a change in the seafloor  
571 currents directions that are deflected by the structure. [Rasidah et al. \(2010\)](#) have  
572 noticed the settling of turbulences on the edges of the structure that could be due to  
573 the diffraction of the waves' energy. In the simulations, the observation of the velocity  
574 vectors showed that the current was deflected from the centre of the structure to its  
575 edges and then to the coast. This caused turbulences on the edges that could have  
576 been interpreted as side effects if it was not present in experimental data. In addition  
577 to the direction of the velocity vectors, this effect was seen in the values of these  
578 vectors at both tides (Fig. 5A,B) (Points 8, 14, 15 and 21). Because of the experimental  
579 validation of the control simulations and the one with existing submerged wave  
580 breakers, the results of the other simulations could be considered as first results on  
581 the use of bio-inspired submerged wave breakers.

## 582 4. Discussion

583

### 584 4.1 Existing wave breakers

585 This study aimed to find a solution to one of the main problems of wave-breaker: the  
586 increasing erosion of non-protected areas. When a structure is settled, it protects some  
587 areas by decreasing waves energy and slowing the current on the seafloor but it  
588 reflects some of the swell energy. This reflection increases the current at another place  
589 and that will enhance the erosion in most cases ([Williams et al., 2018](#)). This reflection  
590 was present in the simulation. The speed vectors were changing direction when they  
591 had a contact with the wave-breaker and there were accelerations on the sides of the  
592 structure (EMODnet., 2020). The followed method allows verifying the risk of eroding  
593 non-protected zones by comparing the speed of seafloor currents with and without a  
594 wave-breaker at different places. If a structure caused a general slowdown in current  
595 around and after it, it means that the energy was dissipated and not reflected which  
596 would not increase the erosion in the non-protected areas. On the other hand, if a  
597 model generated accelerations in some zones, it would increase the erosion in these  
598 places and consequently cause a destabilization of the sediment dynamics.

599 The existing models were slowing the current at flood tide, and thus were decreasing  
600 the erosion. There were some little accelerations at some observation points but  
601 nothing that would risk causing some major changes. At ebb tide, however, the  
602 accelerations areas ( $+0.3$  or  $+0.7 \text{ m}\cdot\text{s}^{-2}$ ) were destabilizing the sedimentary cell. These  
603 accelerations would cause the increase of erosion in several areas and this could  
604 change the morphology of the beach. For example, the huge acceleration just behind  
605 the longshore bar could move faster this structure in the medium or long term. Even if  
606 this bar was considered as fixed because of the 45 seconds duration of the simulation,  
607 it is important to understand that this structure is moving naturally with the tides and  
608 the swell. These results went in the direction of previous studies which claimed that  
609 building offshore structures as wave-breaker increase the erosion of some areas.

610

### 611 4.2 Nest-inspired wave breakers

612 The nest-inspired wave breakers had diverse behaviour and could cause a slowdown  
613 of the seafloor current in some areas, depending on the tide. However, every model  
614 was causing accelerations in some areas and the average slowdown was not  
615 consequent. These accelerations could go up to  $+0.5 \text{ m.s}^{-2}$ . This value, compared to  
616 the size of sand particles using the Hjulström diagram ([Hjulström, 1935](#)), was very high  
617 and even with a base value of  $0.0 \text{ m.s}^{-1}$ , the acceleration would be enough to erode  
618 and move sand particles. No model had shown a general slowdown at the ebb and  
619 flood tide. Finally, these really large structures (285 m long) were not causing an  
620 average slowdown that would be relevant to a use in real conditions. For these  
621 reasons, none of the nest-inspired models tested seemed to be a solution to manage  
622 the general coastal setback.

623

#### 624 4.3 Mangrove-inspired wave breakers

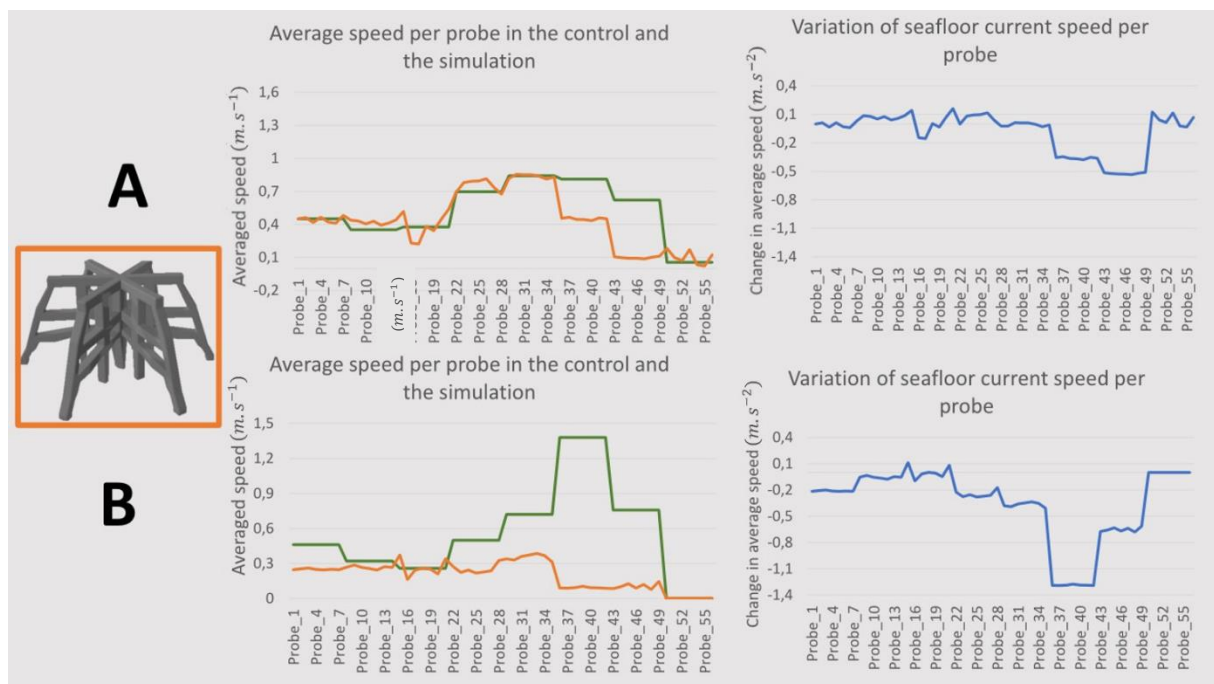
625 The mangrove-inspired immersed wave breakers had diverse behaviours but they  
626 seemed way more interesting than the nest-inspired ones. They all showed a general  
627 slowing that went up to  $-0.40 \text{ m.s}^{-2}$  at ebb tide. Above all, these models presented no  
628 zones with important accelerations. At flood tides, there had been some small  
629 accelerations (less than  $+0.2 \text{ m.s}^{-2}$ ) between lines one and five. A general slowdown  
630 of the seafloor current meant decreasing erosion and increasing sedimentation.  
631 Therefore, these results could show a solution to the swelling erosion.

632 To estimate how efficient mangrove-inspired wave breakers could be, two parameters  
633 were considered: the number of rows and the density of roots (Fig.7 and Fig.8).  
634 Setting up two lines of artificial mangroves seemed to be the best solution (Fig.8)  
635 because it caused the most important slow down at both tides for most of the  
636 observation points. Two consecutive rows would cause the most important decrease  
637 to the swell erosion and could slow coastal setback in the Bay of Biscay. Changing the  
638 number of vertical roots had not caused an important change at flood tide but at ebb  
639 tide, with the four-roots-per-axis model, the seafloor current speed was always under  
640  $0.4 \text{ m.s}^{-1}$  (Fig.10). Because this model didn't seem to create accelerations zones  
641 around the structure and generate a global seafloor current slowdown, it could be the  
642 most efficient to answer the problem of coastal setback.

643 By dissipating the energy of the wave, the impact on coastal sediments should be  
644 decreased in a meaningful proportion, decreasing the general coastal erosion. The  
645 efficiency of vegetation in dissipating wave energy, especially in mangrove settings,  
646 was established by numerous studies ([Dalrymple et al., 1984](#)). More recently, [Zhang et al. \(2020\)](#)  
647 applied Dalrymple's model to estimate how the wave attenuation was  
648 changing depending on the mangrove's structure. Overall a decrease in wave height  
649 is observed in any case of mangrove situation, which is corroborated by other studies  
650 ([Phan et al., 2014](#)). Most of those studies ([Mendez et al. , 2004](#)) occur in a study area  
651 that is similar to the conditions of our study: fine sediments, depth below 10m, and  
652 similar wave speed. However, it is important to wonder if some scale effects can also  
653 be at play and impact sediment erosion around the wave breaker. It is important to be  
654 aware of the turbulence that could be generated by the roots-like structure at a smallest  
655 scale than the experimental scale used in the study. Recent papers on sediment

656 transport in vegetated channels show that, especially in mangrove-like areas, local  
 657 turbulence can be generated by the presence of roots study (Yang and Heidi, 2018).  
 658 These turbulences could create local vortex, able to lift up particles and affect the  
 659 bedload. This effect should be considered for former experimentations in this particular  
 660 setting. Other recent studies tend to induce that erosion in sand environments in  
 661 mangrove forests should consider near-bed turbulent energy instead of general  
 662 velocity (Norris et al., 2021). All those physical mechanisms should be considered  
 663 when studying the impact of mangrove-like wave breakers and before  
 664 implementation.

665 Fig.10. (Full page width)



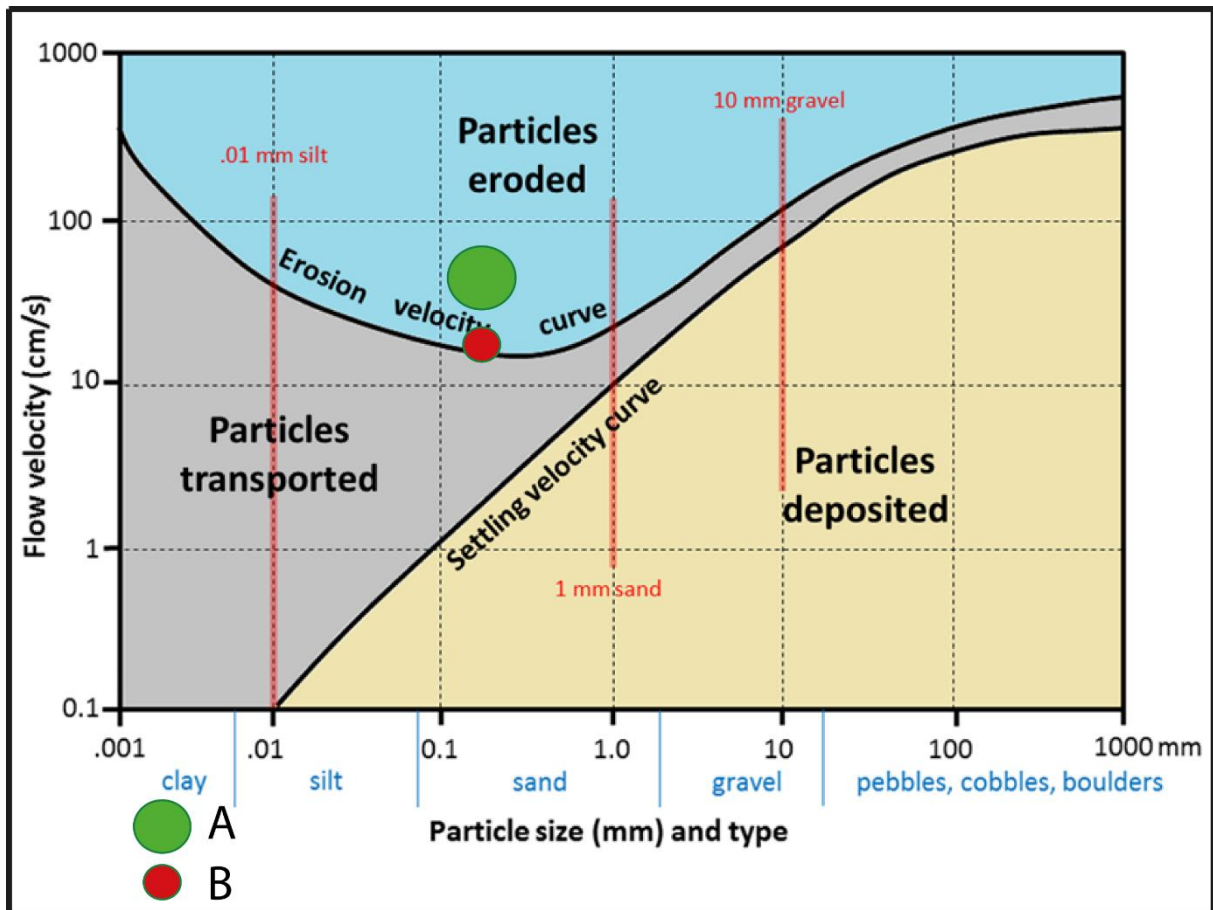
666

#### 667 4.4 Efficiency comparison

668 In order to compare the efficiency of the models, the average speeds of all simulations  
 669 have been placed in the Hjulström-Sundborg diagram. The average particle size in the  
 670 Bay of Biscay is 0.15 mm. This means that even if the size of the particles changes  
 671 along the coastline and along the profile of the beach, this size helps to understand the  
 672 general behaviour of the particles. All the points, no matter the tide or the model used,  
 673 were placed in the green circle (Fig.11 A). The only point that was out of it is the  
 674 average speed of the four-roots-per-axis mangrove at ebb tide (Fig.11 B). Even if the  
 675 seafloor current speed could be divided by three (0.63 to 0.23 m.s<sup>-1</sup>), all the values  
 676 were really close on the diagram because of the logarithmic scale.

677

678 Fig.11 (small column size)



679

680 The value of a speed vector with two dimensions was calculated to combine results at  
 681 both tides to class the efficiency of the wave breakers. The vector's coordinates were  
 682 the average speed at flood tide and the average speed at ebb tide. The length of this  
 683 vector has been calculated with the following equation (Eq. 5). The lower the average  
 684 speed is, the better because it means a more important decrease in the swell erosion.  
 685 On the one hand, this method is interesting because even if a wave-breaker creates  
 686 an important slowdown at one tide, it will need to be performant at both tides to get the  
 687 lowest average speed possible. On the other hand, if it allows estimating the efficiency  
 688 of the model, this parameter doesn't give data about the increasing erosion of non-  
 689 protected areas.

690

691

$$Eq.5: AS = ((ASFT)^2 + (ASET)^2)^{1/2}$$

692

693 With *AS* the average speed, *ASFT* the average speed at flood tide, and *ASET* the  
 694 average speed at ebb tide. The three parameters are in  $m.s^{-1}$ .

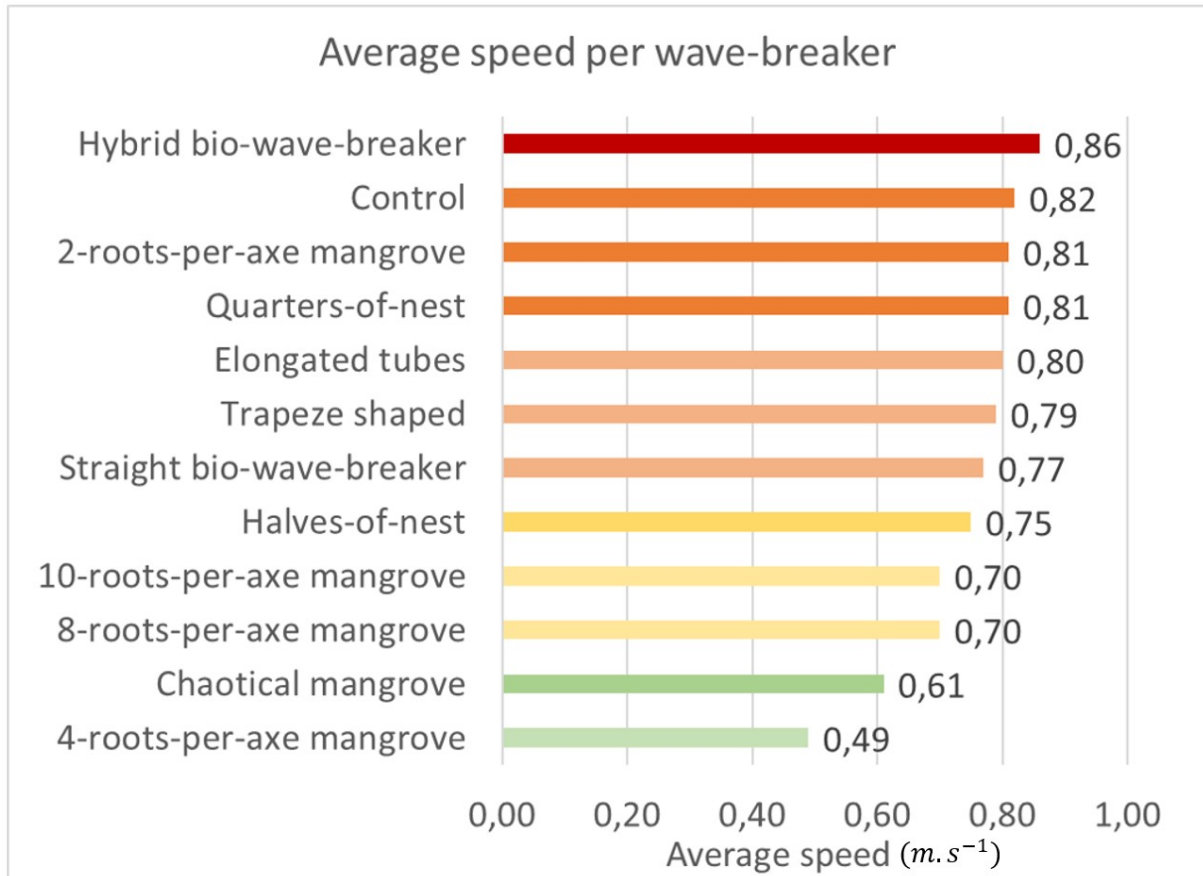
695

696 When the average speed for all the wave breakers was compared on a graph (Fig.12),  
 697 it was very clear that the hybrid bio-wave-breaker is counter-productive and that the  
 698 best set-up was two rows of the 4-roots-per-axis mangroves that had an average speed  
 699 of  $0.49 m.s^{-1}$ . The control value was  $0.82 m.s^{-1}$ . Because of this and of the fact that this  
 model didn't create important accelerations at any observation points, this set-up

700 seemed to be the optimum one. Furthermore, it showed that the nest-inspired wave  
701 breakers didn't reduce a lot the average speed in addition to increasing the erosion in  
702 some non-protected areas.

703

704 Fig.12 (small column size)



705

706 It could have been interesting to compare these seafloor current speed results with the  
707 height of waves when they break down and the distance to the wave-breaker.  
708 Collecting these values was not possible because of the meshing size in the simulation.  
709 The computer was able to calculate all the fluids values in every mesh, but it couldn't  
710 give The a wave picture we could measure precisely. Doing smaller simulations with a  
711 smaller meshing size could be a prospect of a future study.

712

#### 713 4.5 Limits and prospects

714

715 It is important to notice that all these results were given by numerical simulations so  
716 there are a few limits to consider. Firstly, the mesh was 1 m large in all the simulations  
717 and 0.25 m large around the wave breakers. The results could have been different with  
718 a smaller meshing size. It was not possible to use a smaller one because the software  
719 would not have been able to generate the Lattice domain. Then, the length of the  
720 simulations was 45 seconds and they took between 10 and 19 hours to be computed.

721 To study a global phenomenon such as erosion, definitive results couldn't be  
722 calculated and given without an experiment lasting several days.

723 Finally, the stability parameter was not optimum. This parameter in a numerical  
724 simulation depends on three conditions. If one is not satisfied somewhere in the  
725 generated domain, the parameter will reach 1.00 and higher. In the simulations, it was  
726 most of the time under 0.06 but sometimes, reach 0.2. The most important in a  
727 numerical simulation is to keep it between 0 and 1 but the lower this value is, the better.

728 Simulations' results need to be converging and to be verified experimentally to be  
729 completely correct. The convergence is given by the software used (Xflow®2020). The  
730 validation criteria was validated with the comparing of simulation results and  
731 experimental results found in the scientific literature. The next step will be to validate  
732 the results with test bench experiments. Another step could be to model a particular  
733 georeferenced beach with details and to make simulations with precise swell and tide  
734 data to obtain results about the possibility of the implementation of those structures in  
735 the reality.

736 Other prospects could be to use these bio-wave-breaker shapes in other software to  
737 study the sedimentary outflow, to make larger-scale simulations with more than one  
738 wave-breaker. It could be to make smaller and precise simulations to study the  
739 behaviour of the current when it passes through a mangrove-shaped element, to make  
740 simulations with a more complex beach shape. Another prospect could be to take one  
741 particular beach, to modelize it with details in 3D and to run simulations with precise  
742 swell data to obtain results about a specific case. It has also been shown by many  
743 authors that it is possible to use artificial reefs as wave breakers and to use wave  
744 breakers as artificial reefs. However, in order to make artificial reefs specific materials  
745 need to be used (Frihy et al., 2004; Düzbastılar. F. O. and Şentürk. U., 2009.;  
746 Murakami and Maki, 2011). This article does not consider the material composition of  
747 the wave breaker, therefore, the possibility of making artificial reef has not been  
748 studied.

## 749 5. Conclusions

750

751 This paper aims to suggest bio-inspired wave breakers as a proof of concept in order  
752 to reduce coastal setback and discuss about risks and opportunities of biomimicry  
753 solutions. Biomimicry isn't a goal in itself but rather a potential solution for modern  
754 problems, keeping in mind that all imitations are not useful. The results have shown  
755 the problems generated by existing models and especially the increasing erosion in  
756 the non-protected areas. The *Torquigener* nest's imitation was a promising idea but  
757 simulations have shown that these wave-breaker shapes accelerated the current in  
758 some areas. These results are not definitive and will need to be confirmed, but this  
759 idea doesn't seem to bring a solution to the issue of the increasing erosion of the non-  
760 protected areas.

761 On the other side, the imitation of the mangroves showed interesting results. Both  
762 chaotical and symmetrical shapes caused an important general slowdown at ebb tide  
763 and an average slowdown at flood tide. The best set-up was two lines of a symmetrical

764 model with four vertical roots by axis. This set-up could be perfected with a generative  
765 design study and experimental data with a bench test to confirm simulations' results. It  
766 would be interesting to make an economical study to see if the implementation of this  
767 type of bio-wave breakers could be possible to solve the problem of coastal setback.

768 This paper built upon the idea that nature could give inspirations to solve natural  
769 problems. Even so, all the inspirations found in nature are not a way to deal with these  
770 problems. This study was set up in a mesotidal area. These results have been  
771 generated with general parameters that could feat with the Bay of Biscay in France. It  
772 could be different in the case of a precise location with detailed data. Furthermore, only  
773 the swash and the backwash have been studied. Drift currents have not been  
774 considered and could change the potential efficiency of these bio-wave breakers.

## 775 Credit author statement

776

777 **Corentin Thomas:** Conceptualization, Methodology, Software, Formal analysis,  
778 Investigation, Writing - Original Draft. **Victor Lieunard:** Investigation, Designing  
779 CATIA® Models, Writing - Review & Editing. **Baptiste Oudon:** Simulation, Writing –  
780 Review & Editing. **Olivier Bain:** Validation, Writing - Review & Editing. **Rejanne Le**  
781 **Bivic:** Validation, Writing - Review & Editing. **Arnaud Coutu:** Validation, Writing -  
782 Review & Editing, Supervision, Project administration

## 783 Acknowledgements

784

785 The authors gratefully thank Dassault Systèmes Foundation for the financing, GéoLab  
786 of UniLaSalle Beauvais for the support provided for this work and all the students who  
787 previously worked on bio-inspired simulation subjects: J. M. Vient, C. Adam and L.  
788 Donovan, M. Arnaud and J. Michel.

## 789 References

790

791 Anthony, E.J., 2004. Sediment dynamics and morphological stability of estuarine  
792 mangrove swamps in Sherbro Bay, West Africa. *Marine Geology, Material Exchange*  
793 *Between the Upper Continental Shelf and Mangrove Fringed Coasts with Special*  
794 *Reference to the N. Amazon-Guianas Coast* 208, 207–224.  
795 <https://doi.org/10.1016/j.margeo.2004.04.009> .

796 Aubie, S., & Tastet, J. P. (2000). Coastal erosion, processes and rates: an historical  
797 study of the Gironde coastline, southwestern France. *Journal of Coastal Research*,  
798 756-767

799 Balouin, Y., Longueville, F., Colombet, Y., 2016. Video assessment of nearshore and  
800 beach evolution following the deployment of a submerged geotextile wave breaker.  
801 *Journal of Coastal Research, Proceedings of the 14th International Coastal*  
802 *Symposium (Sydney, Australia) Special Issue*, 617–621. [https://doi.org/10.2112/SI75-](https://doi.org/10.2112/SI75-124.1)  
803 [124.1](https://doi.org/10.2112/SI75-124.1)

804 Boulet, D., Giunta Fornasin, M.E., Heurtefeux, H., 2018. Modes de gestion et  
805 responsabilités des ouvrages de lutte contre l'érosion et la submersion marine en  
806 Occitanie. DOI : 10.5281/zenodo.2222442 .

807 Brivois, O., Idier, D., Thiébot, J., Castelle, B., Le Cozannet, G., & Calvete, D. (2012).  
808 On the use of linear stability model to characterize the morphological behaviour of a  
809 double bar system. Application to Truc Vert beach (France). *Comptes Rendus*  
810 *Geoscience*, 344(5), 277-287.

811 Butel, R., Dupuis, H., & Bonneton, P. (2002). Spatial variability of wave conditions on  
812 the French Atlantic coast using in-situ data. *Journal of Coastal Research*, (36  
813 (10036)), 96-108.

814 Carpentier, L., Brosselard-Faidherbe, F., 1986. Influence de la période de la houle  
815 sur la stabilité des digues à talus. *La Houille Blanche* 371–375.  
816 <https://doi.org/10.1051/lhb/1986039> .

817 Castelle, B., Bonneton, P., 2006. Modelling of a rip current induced by waves over a  
818 ridge and runnel system on the Aquitanian Coast, France. *C. R. Geoscience* 338  
819 (10), 711–717.

820 Cerc., 1984. Shore Protection Manual. Coastal Engineering Research Center, US  
821 Army Engineer Waterways Experiment Station, Vicksburg, MS.

822 Charles, E., Idier, D., Thiébot, J., Le Cozannet, G., Pedreros, R., Ardhuin, F., Planton,  
823 S., 2011. Present wave climate in the Bay of Biscay: spatio- temporal variability and  
824 trends from 1958 to 2001. *J. Climate*, [http:// dx.doi.org/10.1175/JCLI-D-11-00086.1](http://dx.doi.org/10.1175/JCLI-D-11-00086.1).

825 Chen, S., Doolen, G.D., 1998. Lattice Boltzmann Method for Fluid Flows. *Annual*  
826 *Review of Fluid Mechanics* 30, 329–364.  
827 <https://doi.org/10.1146/annurev.fluid.30.1.329>

828 Cho, K.-J., Wood, R., 2016. Biomimetic Robots, in: Springer Handbook of Robotics,  
829 Springer Handbooks. Springer International Publishing, Cham, pp. 543–574.  
830 [https://doi.org/10.1007/978-3-319-32552-1\\_23](https://doi.org/10.1007/978-3-319-32552-1_23)

831 Church, J.A.; P.U. Clark, A. Cazenaze, J.M. Gregory, S. Jevrejeva, A. Levermann,  
832 M.A. Merrifield, G.A. Milne, R.S. Nerem, P.D. Nunn, A.J. Payne, W.T. Pfeffer, D.  
833 Stammer, and A.S. Unnikrishnan, 2013: Sea level change. *Climate Change 2013:*  
834 *The Physical Science Basis. Contribution of Working Group I to the Fifth Assessment*  
835 *Report of the Intergovernmental Panel on Climate Change.*

836 Dalrymple, Robert A., James T. Kirby, and Paul A. Hwang., 1984. Wave diffraction  
837 due to areas of energy dissipation. *Journal of waterway, port, coastal, and ocean*  
838 *engineering* 110.1: 67-79.

839 Dassault Systèmes, 2021. Xflow 2021 User Guide.

840 Delage, G., 1954. Using a breakwater for beach protection. *Coastal Engineering*  
841 *Proceedings* 35–35. <https://doi.org/10.9753/icce.v5.35> .

842 Dodet, G., Bertin, X., Bouchette, F., Gravelle, M., Testut, L., Wöppelmann, G., 2019.  
843 Characterization of Sea-level Variations Along the Metropolitan Coasts of France:

844 Waves, Tides, Storm Surges and Long-term Changes. *Journal of Coastal Research*  
845 88, 10–24. <https://doi.org/10.2112/SI88-003.1>

846 Dupuis, H., Michel, D., Sottolichio, A., 2006. Wave climate evolution in the bay of  
847 biscay over two decades. *J. Mar. Syst.* 63, 105–114.

848 EMODnet, Mean depth full coverage, 2020 version, 2020, [https://portal.emodnet-](https://portal.emodnet-bathymetry.eu/)  
849 [bathymetry.eu/](https://portal.emodnet-bathymetry.eu/) (accessed 23 September 2021).

850 Düzbastılar. F. O., Şentürk. U., 2009. Determining the weights of two types of  
851 artificial reefs required to resist wave action in different water depths and bottom  
852 slopes. *Ocean Engineering*, vol. 36, pp. 900–913.

853 Earle, S., 2015. *Physical Geology*, 1st ed. BCcampus.  
854 <https://opentextbc.ca/geology/> (accessed 18 January 2022).

855 Everett, T., Chen, Q., Karimpour, A., Twilley, R., 2019. Quantification of Swell Energy  
856 and Its Impact on Wetlands in a Deltaic Estuary. *Estuaries and Coasts* 42, 68–84.  
857 <https://doi.org/10.1007/s12237-018-0454-z>

858 Frihy, O. E., El Ganaini, M. A., El Sayed. W. R., Iskander. M. M., 2004. The role of  
859 fringing coral reef in beach protection of Hurghada, Gulf of Suez, Red Sea of Egypt.  
860 *Ecological Engineering*, vol. 22, no. 1, pp. 17–25.

861 Grondeau, M., Mercier, P., Guillou, S., Mear, Y., Poizot, E., n.d., 2016. Quelle  
862 turbulence ambiante pour la simulation numérique LBM-LES d'un environnement  
863 hydrolien? 11. <http://website.ec-nantes.fr/actesjh/images/15JH/Articles/grondeau.pdf>  
864 (accessed 23 September 2021).

865 Hay, C.C., Morrow, E., Kopp, R.E., Mitrovica, J.X., 2015. Probabilistic reanalysis of  
866 twentieth-century sea-level rise. *Nature* 517, 481–484.  
867 <https://doi.org/10.1038/nature14093>

868 Hegde, A.V., 2010. Coastal erosion and mitigation methods – Global state of art.  
869 *INDIAN J. MAR. SCI.* 39.

870 Heubes, D., Bartel, A., Ehrhardt, M., 2013. An introduction to Lattice-Boltzmann  
871 methods. *Novel Trends in Lattice-Boltzmann Methods - Reactive Flow,*  
872 *Physicochemical Transport and Fluid-Structure Interaction* 3, 3–30.  
873 <https://doi.org/10.1016/j.cam.2013.09.019> .

874 Hjulström, F., 1935. Studies of Morphological Activity of Rivers as Illustrated by the  
875 River Fyris. *Bulletin of the Geological Institute University of Uppsala*, 25, 221-527

876 Hong Phuoc, V.L., Massel, S.R., 2006. Experiments on wave motion and suspended  
877 sediment concentration at Nang Hai, Can Gio mangrove forest, Southern Vietnam.  
878 *Oceanologia* 48.  
879 [https://www.researchgate.net/publication/26473444\\_Experiments\\_on\\_wave\\_motion\\_](https://www.researchgate.net/publication/26473444_Experiments_on_wave_motion_and_suspended_sediment_concentration_at_Nang_Hai_Can_Gio_mangrove_forest_Southern_Vietnam)  
880 [and\\_suspended\\_sediment\\_concentration\\_at\\_Nang\\_Hai\\_Can\\_Gio\\_mangrove\\_forest](https://www.researchgate.net/publication/26473444_Experiments_on_wave_motion_and_suspended_sediment_concentration_at_Nang_Hai_Can_Gio_mangrove_forest_Southern_Vietnam)  
881 [\\_Southern\\_Vietnam](https://www.researchgate.net/publication/26473444_Experiments_on_wave_motion_and_suspended_sediment_concentration_at_Nang_Hai_Can_Gio_mangrove_forest_Southern_Vietnam) (accessed 23 September 2021)

882 Hornack, M., 2011. Wave reflection characteristics of permeable and impermeable  
883 submerged trapezoidal breakwaters - ProQuest (PhD thesis), Clemson University.

884

885

886 Horstman, E.M., Dohmen-Janssen, C.M., Narra, P.M.F., van den Berg, N.J.F.,  
887 Siemerink, M., Hulscher, S.J.M.H., 2014. Wave attenuation in mangroves: A  
888 quantitative approach to field observations. *Coastal Engineering* 94, 47–62.  
889 <https://doi.org/10.1016/j.coastaleng.2014.08.005> .

890 Isebe, D., Bouchette, F., MOHAMMADI, B., Azerad, P., Lambert, A., BUJAN, N.,  
891 Grasso, F., MICHALLET, H., 2008. Une nouvelle approche pour la protection des  
892 plages : Application à la plage du Lido de Sète.  
893 <https://doi.org/10.5150/jngcgc.2008.025-l>

894 Jamshed, S., 2015. Introduction to CFD, in: *Using HPC for Computational Fluid*  
895 *Dynamics*. pp. 1–20. <https://doi.org/10.1016/B978-0-12-801567-4.00001-5> .

896 Kawase, H., Mizuuchi, R., Shin, H., Kitajima, Y., Hosoda, K., Shimizu, M., Iwai, D.,  
897 Kondo, S., 2017. Discovery of an Earliest-Stage “Mystery Circle” and Development of  
898 the Structure Constructed by Pufferfish, *Torquigener albomaculosus* (Pisces:  
899 Tetraodontidae). *Fishes* 2, 14. <https://doi.org/10.3390/fishes2030014> .

900 Kawase, H., Okata, Y., Ito, K., 2013. Role of Huge Geometric Circular Structures in  
901 the Reproduction of a Marine Pufferfish. *Sci Rep* 3, 2106.  
902 <https://doi.org/10.1038/srep02106> .

903 Komar P.D., Inman D.L., 1970. Longshore sand transport on beaches, *J. Geophys.*  
904 *Res.*, 75(30), 5914-5927.

905 Komar., 1979. Beach-slope dependence of longshore current, *Journal of Waterway,*  
906 *Port, Coastal, and Ocean Division, Amer. Soc. Civil Engrs.*, 105(WW4), 460-464.

907 Kopp, R.E., Horton, R.M., Little, C.M., Mitrovica, J.X., Oppenheimer, M., Rasmussen,  
908 D.J., Strauss, B.H., Tebaldi, C., 2014. Probabilistic 21st and 22nd century sea-level  
909 projections at a global network of tide-gauge sites. *Earth’s Future* 2, 383–406.  
910 <https://doi.org/10.1002/2014EF000239>

911 Lacroix, D., Mora, O., de Menthiere, N., Bethinger, A., 2019. La montée du niveau de  
912 la mer : conséquences et anticipations d’ici 2100, l’éclairage de la prospective.  
913 <https://archimer.ifremer.fr/doc/00598/70975/69207.pdf> (accessed 23 September  
914 2021).

915 Larson, M., Kraus, N.C., 1992. Dynamics of Longshore Bars 2219–2232.  
916 <https://doi.org/10.1061/9780872629332.169>

917 Lazure, P., Desmare, S., 2012. Caractéristiques et état écologique - Golfe de  
918 Gascogne-Courantologie.  
919 [https://dcsmm.milieufrance.fr/content/download/4946/file/GDG\\_EE\\_06\\_Courant](https://dcsmm.milieufrance.fr/content/download/4946/file/GDG_EE_06_Courantologie.pdf)  
920 [ologie.pdf](https://dcsmm.milieufrance.fr/content/download/4946/file/GDG_EE_06_Courantologie.pdf) (accessed 23 September 2021).

921 Le Cozannet, G., Lecacheux, S., Delvallée, E., Charles, E., Desramaut, N., Idier, D.,  
922 Krien, Y., Pedreros, R., Oliveros, C., 2011. Influence de la variabilité climatique sur  
923 les vagues dans le golfe de Gascogne 11.

924 Le Cozannet, G., Lecacheux, S., Delvalle´e, E., Desramaut, N., Oliveros, C., Pedreros,  
925 R., 2011. Teleconnection pattern influence in the Bay of Biscay. *J. Climate*,  
926 doi:10.1175/2010JCLI3589.1.

927 Lee, W.K., Tay, S.H.X., Ooi, S.K., Friess, D.A., 2021. Potential short wave  
928 attenuation function of disturbed mangroves. *Estuarine, Coastal and Shelf Science*,  
929 *Mangroves and People: Impacts and Interactions* 248, 106747.  
930 <https://doi.org/10.1016/j.ecss.2020.106747> .

931 Longuet-Higgins M.,1970. Longshore currents generated by obliquely incident sea  
932 waves, *Journal of Geophysical Research*, 75(33), 6778-6789.

933 Masselink, G., Short, A.D., 1993. The effect of tide range on beach morphodynamics,  
934 a conceptual model. *Journal of Coastal Research* 9, 785–800.

935 Massel, S., Gourlay, M., 2000. On the modelling of wave breaking and set-up on  
936 coral reefs. *Coastal Engineering* 39. [https://doi.org/10.1016/S0378-3839\(99\)00052-6](https://doi.org/10.1016/S0378-3839(99)00052-6)

937 Matsuura, K., 2015. A new pufferfish of the genus *Torquigener* that builds “mystery  
938 circles” on sandy bottoms in the Ryukyu Islands, Japan (*Actinopterygii*:  
939 *Tetraodontiformes: Tetraodontidae*). *Ichthyol Res* 62, 207–212.  
940 <https://doi.org/10.1007/s10228-014-0428-5> .

941 Mendez, Fernando J., and Inigo J. Losada., 2004. "An empirical model to estimate  
942 the propagation of random breaking and nonbreaking waves over vegetation  
943 fields." *Coastal Engineering* 51.2: 103-118.

944 Migniot, C., Lorin, J., 1979. Évolution du littoral de la côte des Landes et du Pays  
945 Basque au cours des dernières années. *La Houille Blanche* 65, 267–279.  
946 <https://doi.org/10.1051/lhb/1979026> .

947 Milieumarinfrance, 2020. Gestion intégrée du trait de côte.  
948 [https://www.milieumarinfrance.fr/Nos-rubriques/Actions-concretes/Gestion-integree-](https://www.milieumarinfrance.fr/Nos-rubriques/Actions-concretes/Gestion-integree-du-trait-de-cote)  
949 [du-trait-de-cote](https://www.milieumarinfrance.fr/Nos-rubriques/Actions-concretes/Gestion-integree-du-trait-de-cote) (accessed 23 September 2021).

950 Miller, K.G., Kopp, R.E., Horton, B.P., Browning, J.V., Kemp, A.C., 2013. A geological  
951 perspective on sea-level rise and its impacts along the U.S. mid-Atlantic coast.  
952 *Earth’s Future* 1, 3–18. <https://doi.org/10.1002/2013EF000135>

953 Norris, Benjamin K., Julia, C., Karin, B., Henderson, S, M., 2021. Relating millimeter-  
954 scale turbulence to meter-scale subtidal erosion and accretion across the fringe of a  
955 coastal mangrove forest. *Earth Surface Processes and Landforms* 46.3: 573-592.

956 Pedreros, R., Howa, H., Michel, D., 1996. Application of grain-size-trend analysis for  
957 the determination of sediment transport pathways in intertidal areas. *Mar. Geol.* 135,  
958 35–49.

959 Phan, L.K., van Thiel de Vries, J.S.M., Stive, M.J.F., 2014. Coastal Mangrove  
960 Squeeze in the Mekong Delta. *Journal of Coastal Research* 31, 233–243.  
961 <https://doi.org/10.2112/JCOASTRES-D-14-00049.1> .

962 Rasidah, K.W., Fakhri, I.M., Suhaimi, W.C., Jeyanny, V., Rozita, A., Fadzly, A.K.A.,  
963 2010. Soil physical changes of a coastal mudflat after wave breaker installation 4.

- 964 Repousis, E., Metallinos, A., Memos, C., 2014. Wave Breaking over Submerged  
965 Breakwaters.
- 966 Sabatier, F., Samat, O., Brunel, C., Heurtefeux, H., Delanghe, D., 2009.  
967 Determination of set-back lines on eroding coasts. Example of the beaches of the  
968 Gulf of Lions (French Mediterranean Coast). *Journal of Coastal Conservation* 13, 57–  
969 64. <https://doi.org/10.1007/s11852-009-0062-y>
- 970 Satjaritanun, P., Bringley, E., Regalbuto, J.R., Regalbuto, J.A., Register, J., Weidner,  
971 J.W., Khunatorn, Y., Shimpalee, S., 2018. Experimental and computational  
972 investigation of mixing with contra-rotating, baffle-free impellers. *Chemical*
- 973 S  n  chal, N., Gouriou, T., Castelle, B., Parisot, J. P., Capo, S., Bujan, S., & Howa,  
974 H. (2009). Morphodynamic response of a meso-to macro-tidal intermediate beach  
975 based on a long-term data set. *Geomorphology*, 107(3-4), 263-274.
- 976 Stocker, T.F., D. Qin, G.-K. Plattner, M. 6 Tignor, S.K. Allen, J. Boschung, A. Nauels,  
977 Y. Xia, V. Bex, and P.M. Midgley, Eds. 7 Cambridge University Press, Cambridge,  
978 United Kingdom and New York, NY, USA, 1137– 8 1216.  
979 <http://www.climatechange2013.org/report/full-report/> (accessed 23 September  
980 2021) Sweet, W., Horton, R., Kopp, R., Romanou, A., 2017. Sea level rise.  
981 Publications, Agencies and Staff of the U.S. Department of Commerce.
- 982 Thom, B.G., 1967. Mangrove Ecology and Deltaic Geomorphology: Tabasco, Mexico.  
983 *Journal of Ecology* 55, 301–343. <https://doi.org/10.2307/2257879> .
- 984 Toyoshima, O., Shuto, N., Hashimoto, H., 1966. Wave Run-Up on Coastal  
985 Structures. *Coastal Engineering in Japan* 9, 119–126.  
986 <https://doi.org/10.1080/05785634.1966.11924677> .
- 987 Van Rijn, L.C., 2011. Coastal erosion and control. *Ocean & Coastal Management*,  
988 Concepts and Science for Coastal Erosion Management (Conscience) 54, 867–887.  
989 <https://doi.org/10.1016/j.ocecoaman.2011.05.004> .
- 990 Van Santen, P., Augustinus, P.G.E.F., Janssen-Stelder, B.M., Quartel, S., Tri, N.H.,  
991 2007. Sedimentation in an estuarine mangrove system. *Journal of Asian Earth*  
992 *Sciences, Morphodynamics of the Red River Delta, Vietnam* 29, 566–575.  
993 <https://doi.org/10.1016/j.jseaes.2006.05.011> .
- 994 Vandermeirsch, F., Bonnat, A., Xiaoming, Y., Lazure, P., 2012. Caract  ristiques et  
995   tat   cologique - Golfe de Gascogne-Variation spatio-temporelle de la temp  rature et  
996 de la salinit  . <https://archimer.ifremer.fr/doc/00328/43924/43497.pdf> (accessed 23  
997 September 2021).
- 998 Wen, L., Weaver, J.C., Lauder, G.V., 2014. Biomimetic shark skin: design, fabrication  
999 and hydrodynamic function. *Journal of Experimental Biology* 217, 1656–1666.  
1000 <https://doi.org/10.1242/jeb.097097>
- 1001 Williams, A.T., Rangel-Buitrago, N., Pranzini, E., Anfuso, G., 2018. The management  
1002 of coastal erosion. *Ocean & Coastal Management*, SI: MSforCEP 156, 4–20.  
1003 <https://doi.org/10.1016/j.ocecoaman.2017.03.022> .

- 1004 Wright, L. D., & Short, A. D. (1984). Morphodynamic variability of surf zones and  
1005 beaches: a synthesis. *Marine geology*, 56(1-4), 93-118.
- 1006 Yang, Judy Q., and Heidi M. Nepf., 2018. A turbulence-based bed-load transport  
1007 model for bare and vegetated channels. *Geophysical Research Letters* 45.19: 10-  
1008 428.
- 1009 Zhang, Y., Yang, Y., Yang, K., Tan, X., Sun, X., Leng, B., Zhou, C., Zhu, B., 2020.  
1010 Non-linear wave attenuation quantification model improves the estimation of wave  
1011 attenuation efficiency of mangroves. *Estuarine, Coastal and Shelf Science* 245:  
1012 106927.
- 1013 Figure Captions  
1014 (Colors should be used for every figure)
- 1015 Table 1. Value of the wave breakers' parameters used in the simulations
- 1016 Table 2: Change of the mean water velocity on the probes for the 4 roots per axe  
1017 mangrove wave breakers
- 1018 Fig.1. 2D Profile of the domain and boundary conditions
- 1019 Fig.2. 2D Profile and 3D Model of the beach used in the simulations
- 1020 A. 2D Profile of the beach in the Golfe de Gascogne around Arcachon  
1021 B. 3D Model of the beach with the location of the 8 observation points  
1022 (probes) lines  
1023 C. Location of the beach profile
- 1024 Fig.3. Inspired by the nest wave breakers
- 1025 A. Trapeze-shaped wave-breaker  
1026 B. Elongated tubes wave-breaker  
1027 C. *Torquigener albomaculosus*' nest  
1028 D. First straight bio-inspired wave-breaker  
1029 E. Second straight bio-inspired wave-breaker  
1030 F. Wave-breaker built with quarters of the nest  
1031 G. Wave-breaker built with thirds of the nest  
1032 H. Wave-breaker built with halves of the nest  
1033 I. Wave-breaker with the taller dune facing the sea  
1034 J. Hybrid wave-breaker
- 1035 Fig.4. Inspired by the mangrove wave breakers
- 1036 A. Mangrove scheme  
1037 B. Symmetrical mangrove with eight vertical roots by axis  
1038 C. Symmetrical mangrove with ten vertical roots by axis  
1039 D. Symmetrical mangrove with four vertical roots by axis  
1040 E. Symmetrical mangrove with two vertical roots by axis  
1041 F. Chaotical mangrove
- 1042 Fig.5. Seafloor current speed depending on the existing wave-breaker used

1043 Blue: control seafloor current speed  
1044 Purple: seafloor current speed with the trapeze-shaped wave-breaker  
1045 Yellow: seafloor current speed with the elongated tubes wave-breaker  
1046 A. Results at flood tide  
1047 B. Results at ebb tide

1048 Fig.6. Seafloor current speed depending on bio-wave-breaker used

1049 Blue: control seafloor current speed  
1050 Red: seafloor current speed with the straight bio-wave-breaker (Fig.2 D)  
1051 Purple: seafloor current speed with the quarter-of-nest bio-wave-breaker (Fig.2  
1052 F)  
1053 Green: seafloor current speed with halves-of-nest bio-wave-breaker (Fig.2 H)  
1054 Yellow: seafloor current speed with hybrid wave-breaker (Fig.2 J)  
1055 A. Results at flood tide  
1056 B. Results at ebb tide

1057 Fig.7. Seafloor current speed depending on the roots' density

1058 Blue: control seafloor current speed  
1059 Purple: seafloor current speed with four roots per axis  
1060 Yellow: seafloor current speed with eight roots per axis  
1061 Green: seafloor current speed with ten roots per axis  
1062 A. Results at flood tide  
1063 B. Results at ebb tide

1064 Fig.8. Seafloor current speed depending on the number of lines

1065 Blue: control seafloor current speed  
1066 Purple: seafloor current speed with one line  
1067 Yellow: seafloor current speed with two lines  
1068 Green: seafloor current speed with three lines  
1069 A. Results at flood tide  
1070 B. Results at ebb tide

1071 Fig.9. Variation of seafloor current velocity per probe.4 roots per axe mangrove wave  
1072 breaker simulation with different current orientation

1073 Blue: Seafloor current speed for the 75° simulation  
1074 Orange: Seafloor current speed for the 60° simulation

1075 Gray: Seafloor current speed for the 45° simulation

1076 Yellow: Seafloor current speed for the 30° simulation

1077 Fig.10. Average speeds per observation point (probe)with and without two rows of  
1078 two-vertical-roots-per-axis mangroves

1079 Green: average speed per point in the control simulation

1080 Orange: average speed per point in the simulation with wave-breaker

1081 Blue: average acceleration when the wave-breaker is used

1082 A. Results at flood tide

1083 B. Results at ebb tide

1084 Fig.11. Simulations' average speed in a Hjulström-Sundborg diagram ([Earle, 2015](#);  
1085 [Hjulström, 1935](#))

1086 A: All the simulations except one

1087 B: Simulation at ebb tide of a 4-roots-per-axis mangroves wave-breaker

1088 Fig.12. Average speed per wave-breaker

1089 Green: under 0.65 m.s<sup>-1</sup>

1090 Yellow: between 0.66 and 0.75 m.s<sup>-1</sup>

1091 Orange: between 0.76 and 0.85 m.s<sup>-1</sup>

1092 Red: over 0.86 m.s<sup>-1</sup>